09

STIF

III

AED R-4011
Issued: May 31, 1974

E74-10635
CR-138809

Meteorological Utility of High Resolution Multi-Spectral Data

Final Report

Principal Investigator:
John M. Danko
PR-324

"Made available under NASA sponsorship in the interest of early and wide dissemination of Earth Resources Survey Program information and without liability for any use made thereof."

Prepared for
National Aeronautics and Space Administration
Goddard Space Flight Center
Greenbelt, Maryland 20771

Original photography may be purchased from:
EROS Data Center
10th and Dakota Avenue
Sioux Falls, SD 57198

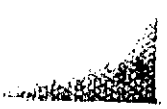

RCA

Prepared by
RCA Government and Commercial Systems
Astro-Electronics Division, Princeton, New Jersey 08540

1169A

RECEIVED
JUN 27 1974
SIS/902.6

(E74-10635) METEOROLOGICAL UTILITY OF HIGH RESOLUTION MULTI-SPECTRAL DATA Final Report (Radio Corp. of America) 68 p HC $6.50 CSCL 04B
N74-28869
G3/13 Unclas 00635

AED R-4011
Issued: May 31, 1974

Meteorological Utility of High Resolution Multi-Spectral Data

Final Report

Principal Investigator:
John M. Danko
PR-324

Prepared for
National Aeronautics and Space Administration
Goddard Space Flight Center
Greenbelt, Maryland 20771

Original photography may be purchased from:
EROS Data Center
10th and Dakota Avenue
Sioux Falls, SD 57198

Prepared by
RCA Government and Commercial Systems
Astro-Electronics Division, Princeton, New Jersey 08540

TABLE OF CONTENTS

		Page
1.0	SUMMARY	1
2.0	GENERAL EXPERIMENT DESCRIPTION	2
	2.1 Background	2
	2.2 Objectives	4
	2.3 Approach	4
	2.3.1 Selection of ERTS MSS Frames	5
	2.3.2 Use of NOAA-2 Imagery	6
	2.4 Data Handling Overview	7
3.0	RESOLUTION REDUCTION	7
	3.1 Experimental Method	7
	3.1.1 Experimental Facility	7
	3.1.1.1 Experimental Parameters	11
	3.1.2 Photographic Parameters	13
	3.1.3 Processing Algorithms	
	3.1.3.1 One-Eighth Nautical Mile Simulation	14
	3.1.3.2 One-Fourth Nautical Mile Simulation	14
	3.1.3.3 One-Half Nautical Mile Simulation	16
	3.1.3.4 One Nautical Mile Simulation	16
	3.1.3.5 Aliasing	21
	3.2 Results	21
	3.2.1 Frames 1098-15141 through-15150 (Figures A-1 and 3.9)	22
	3.2.2 Frames 1100-15325 through-15343 (Figures A-2A and B; and Figures 3.13A & B)	22
	3.2.3 Frames 1100-15284 through-15293 (Figures A-3 and 3.14)	27
	3.2.4 Frames 1099-17020 through 1099-17025 (Figures A-4 and 3.17)	27
	3.2.5 Frames 1099-17040 through-17045 (Figures A-5 and 3.18)	34
	3.2.6 Frames 1121-17324 - 17321 (Figures A-6 and 3.19)	34
	3.2.7 Frames 1070-16034, -16041 (Figure A-7)	34
	3.2.8 Frames 1099-15184 through -15193 (Figure A-8)	37
	3.2.9 Frames 1182-16224, -16231 (Figure A-9 and 3.20)	37

PRECEDING PAGE BLANK NOT FILMED

TABLE OF CONTENTS (Continued)

		Page
3.2.10	Frames 1088-16055, -16061 (Figure A-10)	42
3.2.11	Frames 1173-15362 (Figure A-11)	42
3.2.12	Frame 1173 (Figure A-12)	42
3.2.13	Frames 1003-14485, -14482 (Figure A-13)	43
3.2.14	Frame 1096-15092 (Figure A-14)	43
3.2.15	Frames 1062-15195, -15202 (Figure A-15)	43
3.2.16	Frames 1127-18064 through -18073 (Figure A-16)	44
3.2.17	Frames 1010-20290 through -20295 (Figure A-17)	44
3.2.18	Frames 1004-16322, -16324 (Figure A-18)	44
3.2.19	Frames 1064-15324 through -15333 (Figure A-19)	44
3.2.20	Frames 1099-15211 through -15220 (Figure A-20)	44
4.0	SPECTRAL INTERVAL UTILITY ANALYSIS	44
4.1	Experimental Methods	44
4.2	Results	48
APPENDIX A -	Catalog of Degraded MSS Scenes	62

LIST OF ILLUSTRATIONS

Figure		Page
2.1	Data Handling Block Diagram	8
2.2	Image Product Flow	9
3.1	Resolution Reduction Processing	10
3.2	Read and Write Aperture Modulation Transfer Function (MTF's)	12
3.3	Density Transfer Characteristic of the Color Scanner	13
3.4	Resolution Reduction Algorithms	15
3.5	Processing MTF's Theoretical Sine Wave Response on Axis	17
3.6	MTF of Reduction Resolution Output Imagery	18
3.7	Simulation of 4X4 Average Process	19
3.8	Interpolation Process	20
3.9	Frames 1098-15141-15150	23
3.10	Surface Chart 10/29/1200Z	24
3.11	Spacecraft Chart 10/31/12Z	25
3.12	VHRR Image Oct. 31, 1972 (0.6 - 0.7μ)	26
3.13a	Frames 1100-15325-15343	28
3.13b	VHRR Enlargement 1/2 nmi	29
3.14	Frames 1100-15284-15293	30
3.15	VHRR Image Oct. 31, 1972 (0.6 - 0.7μ)	31
3.16	Surface Chart 10/30/1200Z	32
3.17	Frames 1099-17020-17025	33
3.18	Frames 1099-17040-17045	35
3.19	Frames 1121-17324-17321	36
3.20	Frames 1182-16224-16231	38
3.21	SR Hemispheric Montage (0.5 - 0.7μ)	39
3.22	VHRR Image 21 Jan. 1973 (0.6 - 0.7μ)	40
3.23	VHRR Image 21 Jan. 1973 (10.5 - 12.5μ)	41
4.1	Sample Densitometer Trace	46
4.2	Sample Densitometer Trace Worksheet	47
4.3	Sample Radiance/Contrast Worksheet	49
4.4	MSS Frame Used for Microdensitometer Recordings for Radiance & Contrast Measurement - Clouds, Land, Mountain Snow -	50
4.5	MSS Frame Used for Microdensitometer Recordings for Radiance & Contrast Measurement - Clouds, Land, Lakes -	51
4.6	MSS Frame Used for Microdensitometer Recordings for Radiance & Contrast Measurement - Clouds, Ice & Water -	52
4.7	MSS Frame Used for Microdensitometer Recordings for Radiance & Contrast Measurement - Cirrus Clouds/Land & Water -	53
4.8	MSS Frame Used for Microdensitometer Recordings for Radiance & Contrast Measurement - Clouds, New/Thin Ice -	54
4.9	MSS Frame Used for Microdensitometer Recordings for Radiance & Contrast Measurement -A/C Contrails Over Land/Water -	55
4.10	MSS Frame Used for Microdensitometer Recordings for Radiance & Contrast Measurement - Clouds/Land & Water -	56
4.11	MSS Frame Used for Microdensitometer Recordings for Radiance & Contrast Measurements - Stratus, Ice -	57

LIST OF ILLUSTRATIONS (Continued)

Figure		Page
4.12	MSS Frame Used for Microdensitometer Recordings for Radiance & Contrast Measurements - Clouds, Land -	58
4.13	MSS Frame Used for Microdensitometer Recording for Radiance & Contrast Measurements - Clouds, Water -	59
4.14	Sample Observation of Variation in Contrast with Spectral Region	60

METEOROLOGICAL UTILITY OF HIGH RESOLUTION MULTISPECTRAL DATA

1.0 SUMMARY

The recent trend in imaging sensors for meteorological satellites is towards higher resolution in multiple spectral intervals. Design concepts for future meteorological sensors include resolutions below 1/2 nautical mile, with several different spectral intervals being proposed to sense reflected solar radiation.

This investigation used the ERTS-1 Multispectral Scanner (MSS) data to evaluate the relationship between meteorological information content of images as a function of image resolution and the spectral interval of the channel. It is hoped that the results of the experiment will aid in the system planning for future operational meteorological satellite systems.

The experiment had two objectives. The primary objective was to evaluate the meteorological information content of imagery in the 0.6 to 0.7μ spectral band at various resolutions. Towards this end, ERTS MSS Band 5 (0.6 - 0.7μ) imagery in 70mm negative format was obtained from the NASA Data Processing Facility (NDPF) and degraded using digital processing techniques. An RCA 70/8802 Color Scanner and associated minicomputer were used to produce images at three levels of reduced resolution. The degraded images were simulations of data acquired by scanning radiometers with a instantaneous-field-of-view of 1/8 nautical mile, 1/4 nautical mile, and 1/2 nautical mile.

The images processed in this portion of the experiment were selected to contain a wide variety of meso-meteorological phenomena, including many different cloud types viewed over various backgrounds. Restrictions on this selection process were imposed by: (1) the inherent problem of searching a vast quantity of data; (2) the small dynamic range of the MSS; and (3) the narrow field-of-view of the MSS relative to the scale of meteorological phenomena. However, twenty-five scenes composed of sixty-five MSS frames were processed producing three reduced resolution images for each scene. Analysis of these scenes led to the following two major conclusions:

(1) When using satellite acquired imagery in the 0.6 - 0.7μ band to determine cloud type, especially in layered conditions, 1/2 nmi resolution data is not adequate for many cases. In the vast majority of the cases examined, the 1/4 nmi resolution data was sufficient for observations of cloud cover. Only in the case of cloud cover over mountain snow was additional information provided by the 1/8 nmi resolution data.

(2) For observations of ice and snow in the 0.6 - 0.7μ band, the resolution requirement appears to be very variable. Sea ice is generally identifiable and differentiable from clouds at 1/2 nmi resolution. Surface snow and lake ice are also generally identifiable at 1/2 nmi resolution. The only exceptions being when partial cloudiness exists over the scene. Then the added surface detail at 1/8 nmi allows for discrimination of the ice and/or snow.

It was not the intent of the investigation to develop new interpretative techniques; consequently, as proposed, a catalog of the various degraded scenes (in positive transparency format) was prepared and is included as Appendix A in this report. Individual meteorological analysts may reference these degraded scenes using individually derived interpretative techniques.

It should be pointed out that the degraded data used in this experiment simulated the direct output of the sensor. In an actual system design, expected degradations to the resolution contributed by the sensor viewing off-vertical, recorders, communications links, displays, and photographic processing should be compensated for by increased sensor resolution such that the final product delivered to the user contains the level of information desired.

The other segment of this experiment had the objective of evaluating various intervals in the reflected solar spectrum from the standpoint of meteorological information content in the image. MSS imagery in Bands 4 (0.5 - 0.6μ), 5 (0.6 - 0.7μ), and 7 (0.8 - 1.1μ) were selected and analyzed. Again, difficulty was encountered in the selection process. Signal saturation resulting from the restricted dynamic range of the MSS channels made it difficult to obtain a wide variety of meteorological phenomena in scenes that could be quantitatively analyzed. Fifteen densitometer traces on ten ERTS MSS scenes were analyzed to obtain contrasts of different meteorological phenomena against various backgrounds. A measurement of each phenomena was made in all three spectral bands. The significant quantitative results can be summarized as follows.

(1) The measured contrast of a variety of cloud types in Band 5 (0.6 - 0.7μ) against land and water backgrounds was in each case more than one-and-one-half times the contrast in Band 4 (0.5 - 0.6μ).

(2) While the high land/water contrast in Band 7 (0.8 - 1.1μ) was observed, the higher albedo of vegetation in Band 7 caused a reduced cloud/land contrast in Band 7 versus that in Band 5. For the cases measured, the quantitative result was that the cloud/land contrasts (where the land contained vegetation, i.e., not predominantly desert or rock) in Band 5 (0.6 - 0.7μ) were in each case more than three times the contrast in Band 7 (0.8 - 1.1μ).

Quantitatively, it can be concluded that for observations of clouds, snow, and ice against any background, a 0.6 - 0.7μ channel provides more contrast and allows for better interpretability than a 0.5 - 0.6μ channel, or even a 0.5 - 0.7μ channel. Furthermore, the results of this experiment indicate that if information provided by a near infrared channel is required, the combining of this energy with that in the visible region will result in a degradation of cloud/land contrasts.

2.0 GENERAL EXPERIMENT DESCRIPTION

2.1 Background

Current and past meteorological satellite sensors have provided imagery made from data collected in various spectral intervals within and near the visible portion of the reflected solar spectrum. The majority of the sensors

in past years have provided these imagery at resolutions of from 2 - 4 nmi. Now, with advancements in the state-of-the-art in sensor technology and with increased capabilities in ground data processing, higher resolution sensors have been developed and are being utilized. This is exemplified by the Very High Resolution Radiometer on NOAA-2 and the imaging radiometer system on the military meteorological satellite; both of which are scanning radiometers with one of the two channels designed to provide high resolution imagery resulting from reflected solar radiation. The other channel in each radiometer is a thermal channel in the infrared window near 11μ. In the case of the VHRR, the sensor's fixed instantaneous-field-of-view (IFOV) results in a resolution element size of 0.5 nmi at the satellite subpoint. The spectral bandpass of the visible channel is from 0.6 - 0.7μ. These parameters are contrasted with those of the Scanning Radiometers (SR), another member of the NOAA-2 sensor complement. The SR visible channel spectral bandpass is 0.5 - 0.7μ and it has an IFOV in this channel which results in a resolution element size of 2.0 nmi at the satellite subpoint. As a result of information gained on the military meteorological satellite system, the decision has been made to change the visible channel's spectral bandpass in the SR on subsequent NOAA spacecraft to 0.45 - 1.1μ.

The two radiometers (SR and VHRR) on the NOAA spacecraft satisfy the operational meteorological satellite system requirement for dual resolution data. The SR provides data having daily global coverage. For this data, a resolution of 2 nmi represents a compromise resulting from the influence of many system elements. Higher resolution data would require more spacecraft tape recorder capacity, a higher bandwidth playback link, more long line capacity for ground transfer of the data from the Command and Data Acquisition stations, and more central processing time in order to produce the final meteorological products. On the other hand, the medium resolution (2 nmi) data apparently provides the meteorological information required from the global product. Major storm systems, tropical storms, and frontal zones can be tracked and their intensity change determined. Most organized cloud patterns are observed in detail sufficient to reflect major features in the upper level flow such as the existence and position of troughs, ridges, and jet streams. Similarly, the cloud formations are used as indicators of surface flow parameters, including spread, curvature and persistence. Other meteorological phenomena such as the distributions of large expanses of snow and ice can be determined to some extent using medium resolution data.

Medium resolution data is also transmitted in real-time from the spacecraft to local users. A direct readout of medium resolution imagery from the SR on the NOAA spacecraft is transmitted continuously.

The high resolution output from the VHRR is also transmitted in real-time continuously; but it is capable of being recorded for only 9 minutes per orbit. The general trend of providing higher resolution imagery to the local forecasters is consistent with the needs of this type of user. The area of interest is generally restricted such that the total data burden is not high. Also, he is generally interested in meso-scale events for which the added detail is useful. The particular cloud type and the existence or absence of multiple layers can be quite significant in short-term local area forecasts.

The VHRR data has provided useful measurements for many different applications, augmenting or supplanting many other methods of data sources. The visible channel has proven to be particularly effective for mapping snow fields and for determining the age, distribution and movement of sea and lake ice.

In light of the recent success for high resolution imagery in the operational meteorological satellite system and the apparent intent to provide this imagery in multiple spectral intervals in the visible region, one could pose two pertinent questions:

(1) Is 0.5 nmi resolution data in the visible region sufficient for operational meteorological purposes?

(2) What is the relative meteorological utility of data acquired in various segments of the visible and near infrared portions of the reflected solar spectrum?

It is the investigation of these two questions towards which this study was directed. The ERTS-1 imagery offers an excellent opportunity to examine the level of meteorological information available in high resolution imagery produced from reflected solar radiation. Also, the complete coverage of the visible and near infrared spectrum by the MSS bands offers the opportunity to quantitatively assess which spectral interval(s) would be desirable for meteorological imagery.

2.2 Objectives

This experiment, as it was proposed, has the following primary and secondary objectives:

Primary: To determine the usefulness of very high resolution imagery by using selected ERTS scenes containing meteorological phenomena in the 0.6 to 0.7μ band at several resolutions.

Secondary: To determine the utility of the 0.6 to 0.7μ region relative to the 0.5 to 0.7μ region and the 0.8 to 1.1μ region for observations of meteorological phenomena.

It was not the objective of the experiment to develop new interpretative techniques. Rather, the ERTS MSS imagery would serve as a vehicle for determining meteorological information content versus resolution in one case and meteorological information content versus spectral interval in the other case. The information resulting from the analysis would then serve as an aid to the specification of requirements for future meteorological satellite sensor systems.

2.3 Approach

The general approach taken in this investigation towards the primary objective was to analyze the meteorological information content of ERTS-1 MSS data in the 0.6 - 0.7μ band for the same scene at several reduced resolutions.

The MSS frames that had been selected and received were examined for suitable meteorological information content. All three spectral bands (MSS 4, 5, and 7) were used in this examination. Suitable scenes, generally composed of from two to five consecutive frames, were selected to undergo resolution reduction.

Only MSS Band 5, 70mm negatives, were processed in the resolution reduction portion of the experiment. The reduced resolution images were simulations of data acquired by scanning radiometers with effective apertures of 1/8 nmi, 1/4 nmi, and 1/2 nmi and were produced for each of the selected scenes. After processing, the four different resolution images (original resolution plus three degraded resolutions) of the same scene were examined. Using NOAA-2 imagery and conventional surface and upper air data when available, the meteorological information content at the various resolutions was assessed.

Since it was not the intent of the investigation to develop new interpretative techniques, the original ERTS scenes were interpreted with the aid of conventional meteorological data and treated as "ground truth" information in the analysis of the reduced resolution images. In general, the MSS images in Bands 4, 5, and 7 plus synoptic surface charts were sufficient to assess the meteorological situation in the scene. Subsequent analysis of the reduced resolution data was then made to determine to what extent the original information was lost.

New techniques for interpreting high resolution imagery for meteorological purposes will no doubt soon be developed by experts in each of the various meteorological fields. Since these techniques can not be anticipated and since there are so many existing interpretative techniques in the wide variety of meteorological oriented disciplines, a catalog of all degraded data has been included in this report. It is hoped that this catalog will be of use to NOAA in assessing their future resolution requirements of satellite acquired imagery.

In satisfaction of the secondary objective, selected scenes containing representative samples of a variety of meteorological phenomena were processed on a scanning microdensitometer. Traces were made from the ERTS-1 MSS 70mm negatives received from NDPF over the same area of a scene in Bands 4, 5, and 7. These traces were then reduced to quantitative measurements of contrast and relative signal strengths in the three spectral regions.

2.3.1 Selection of ERTS MSS Frames

Perhaps the single factor which most hampered the conduct of this investigation was the difficulty in selecting from the tremendous quantity of total ERTS frames, representative samples suitable for processing in this investigation. Several factors contributed to this difficulty. First, the only practical way of selecting scenes was to examine the microfilm catalogs; and since these were not sent out to individual investigators, several trips to the NDPF Browse File had to be made. Even then the actual selection of appropriate scenes was both time consuming and uncertain. The latter effect was caused by the reduced resolution of the microfilm images.

Second, the 100-nmi wide format of the MSS imagery, which is small even by meso-meteorological standards made interpretation of the individual frame content difficult. In an attempt to circumvent this problem, most of the scenes selected for resolution reduction processing were composed of two-to-four consecutive frames.

Finally, the ERTS orbit parameters and the limited dynamic range of the MSS combined to limit the different types of meteorological phenomena which could be obtained in the MSS imagery. Specifically, the mid-morning sun-synchronous orbit of ERTS-1 provided imagery taken at a time when cloud development was generally just beginning. Also, the restricted dynamic range of the MSS resulted in signal saturation by ice, snow, and clouds except at very high latitudes.

Although the experiment was proposed with full recognition of these above factors, their combination presented a problem much more formidable than anticipated. It is no doubt true that every conceivable type of meteorological phenomena has been photographed at least once by ERTS; but finding the particular frames on which they occur is an extremely difficult problem.

Even with the above difficulties, 25 scenes composed of 65 MSS frames were processed in the resolution reduction section of this experiment. These scenes contain a wide variety of meteorological phenomena including many different cloud types and several types of ice and snow. Several of the scenes are obviously saturated in places. These scenes were processed and analyzed since the cloud/background contrast was so high that valid results should have been obtained.

For spectral analysis, however, care was taken to use only those scenes which were not saturated. This restricted the number of samples that could be obtained. Ten frames were analyzed with one to three densitometer traces made for each frame.

2.3.2 Use of NOAA-2 Imagery

It was indicated in the original proposal that NOAA-2 (ITOS-D) VHRR imagery would be used where possible to aid in the investigation. However, NOAA-2 was launched in mid-October 1972, and VHRR data did not become regularly available until late November. Even then several factors reduced the utility of the data for this experiment.

In the first place, the NOAA-2 orbit is a 790-nmi sun-synchronous orbit with a 0900 local descending node time. Because of the ERTS 0942 local descending node time, observations by the two spacecraft of the same point on the earth occur with a temporal separation of approximately 40 minutes. Furthermore, a high resolution display has so far not been used to produce operational VHRR imagery. (Two experimental images, made on the high resolution display in the Direct Readout Ground Station just two weeks after the launch of NOAA-2, were obtained and used in this experiment.) And finally, because of the limited recording capability for VHRR data, only direct readout data over the East Coast of the U.S. up to a latitude of 55° - 60°N is readily available. (Section 3.2.9 of this report does show one particular scene over the full spectrum of image products possible from NOAA-2.)

2.4 Data Handling Overview

Figure 2.1 is a block diagram of the data handling and processing which took place during the conduct of this experiment. Candidate scenes for processing were selected by viewing the microfilm catalogs at the NDPF Browse File. Daily surface and upper air charts from the National Meteorological Center were obtained. When available, photographs made from data obtained by the operational meteorological polar-orbiting satellite were also obtained. The ERTS scenes ordered were screened after receipt to select a representative cross-section of meteorological phenomena for resolution reduction processing. This processing was accomplished on the original 70mm negatives. Also, frames were selected for spectral interval utility processing. After production of the three reduced resolution images, analysis was performed using conventional meteorological data and NOAA satellite photographs. Densitometer traces were run on the original 70mm negatives of those frames selected for spectral analysis.

The resolution reduction process yielded 1st generation negatives. From these, contact positive transparencies were produced and mosaics made. Annotated images produced in the text of this report were made from 3rd generation halftone negatives. The positive transparencies in the catalog in Appendix A are 6th generation images. The photographic processing is depicted by the block diagram in Figure 2.2.

3.0 RESOLUTION REDUCTION

3.1 Experimental Method

In the original proposal for this experiment, it was suggested that the resolution reduction process be accomplished photographically using "slip sheets". However, after submission of the proposal an opportunity to digitally process the data became available. An image processing laboratory at RCA Astro-Electronics Division was developed and became functional. Since the facility consisted of capital equipment, which would present no additional cost to the contract, and since the digital processing procedure could be quantitatively calibrated and controlled, the decision was made after the contract award to utilize this facility and use digital processing methods to produce the degraded images.

3.1.1 Experimental Facility

An RCA 70/8802 Color Scanner and an associated Data General Corporation Super Nova Computer were the main elements of the experimental facility. A system block diagram is shown in Figure 3.1. Specifically, the system is composed of an input read drum on which the ERTS 70mm negatives were placed and read transforming the ERTS image into an analog signal; a 9-bit A/D converter; the Super Nova Computer which performed the required digital filtering; a D/A converter; and the output write drum of the scanner where the processed data stream was used to produce reduced resolution negatives. The color separation capability of the scanner was not used in the experiment.

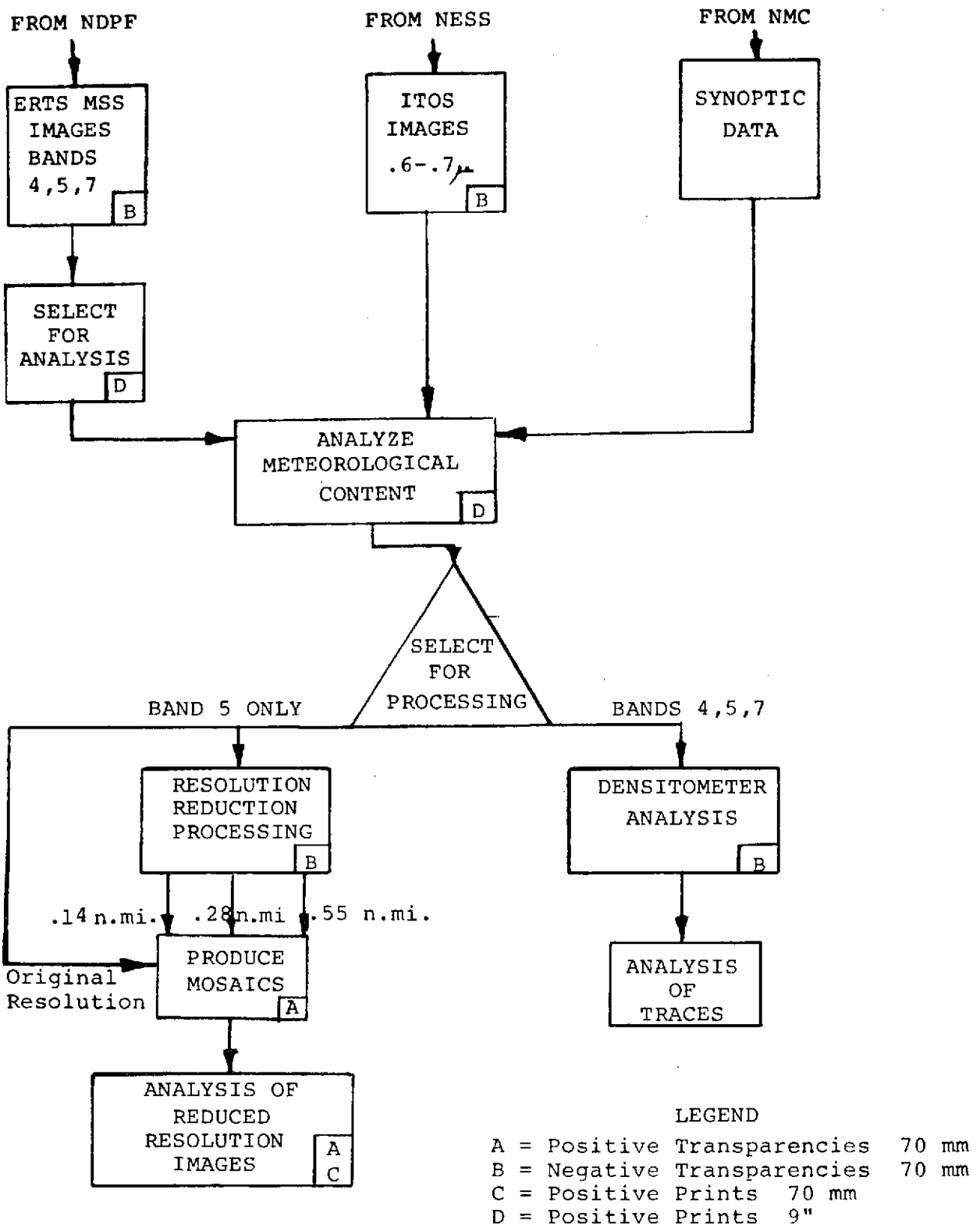

Figure 2.1. Data Handling Block Diagram

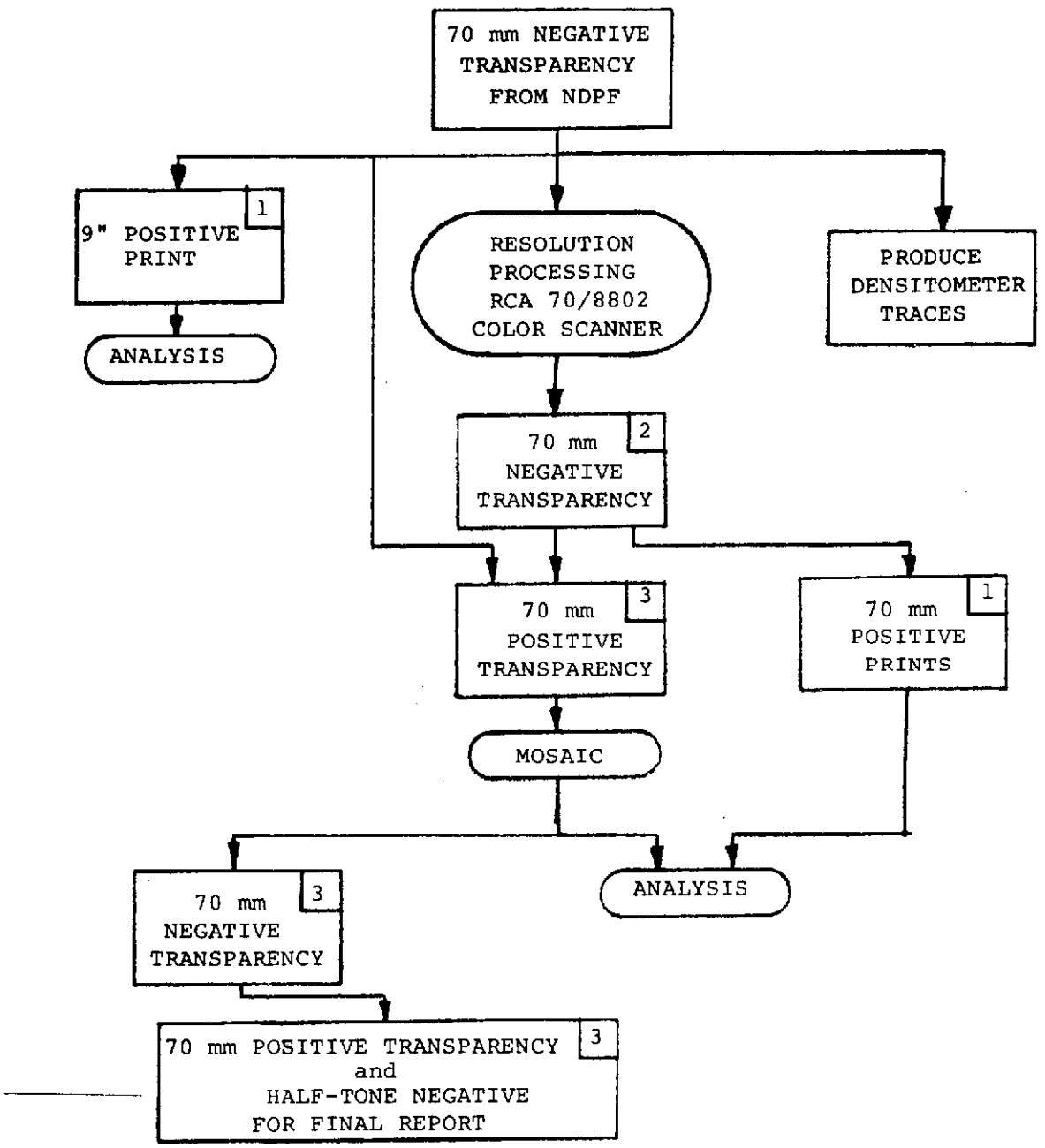

1. KODAK POLYCONTRAST PAPER
DEKTOL DEVELOPER

2. PAKOROL SUPER G-24 PROCESSOR
LUMIERE LUMILTH FILM
and
KODAK 2496 FILM
VERSAMAT A DEVELOPER

3. KODAK 7302 FILM
DEKTOL DEVELOPER

Figure 2.2. Image Product Flow

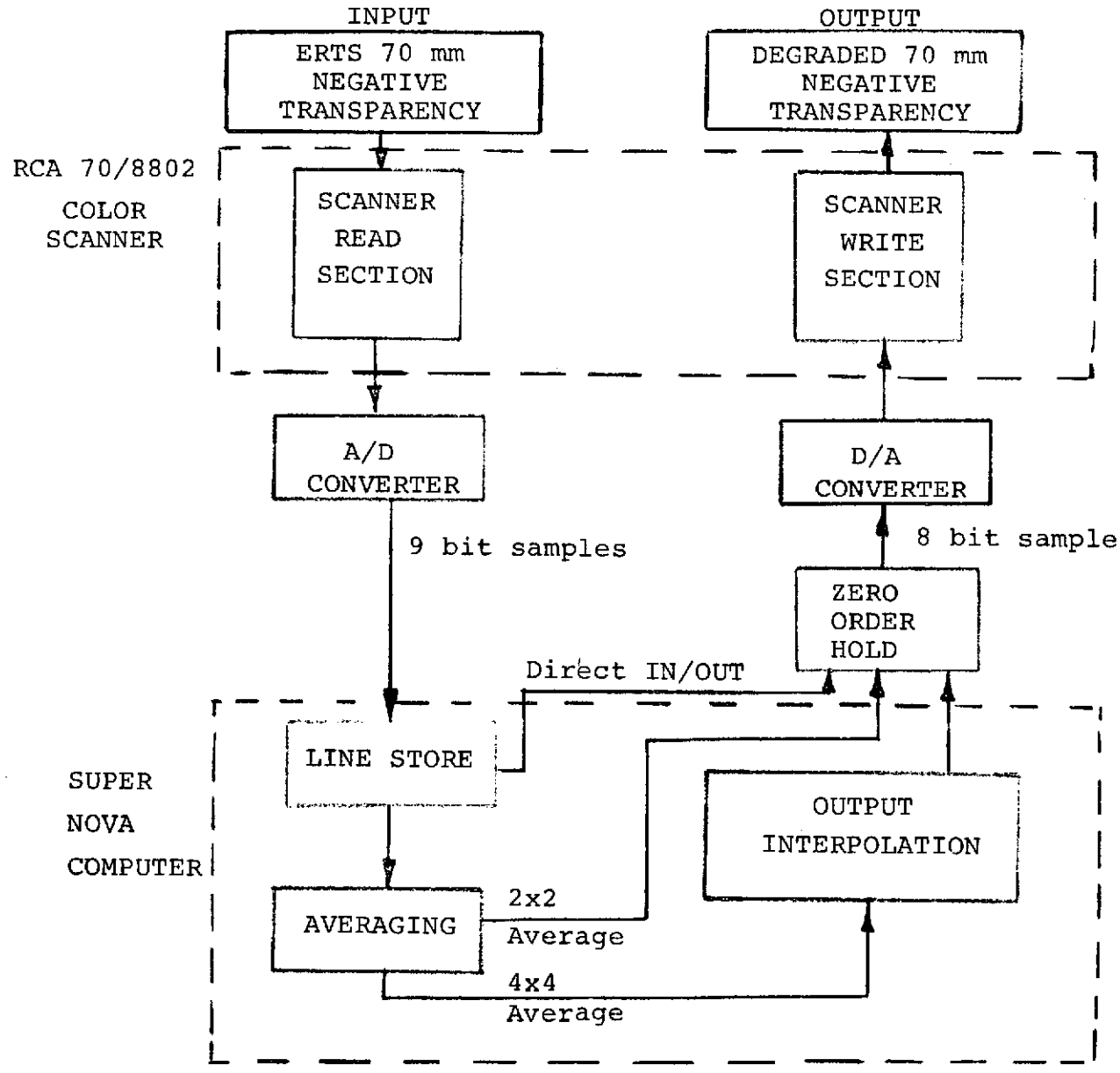

Figure 3.1. Resolution Reduction Processing

3.1.1.1 Experimental Parameters

The major parameters for this facility are shown in Table 3.1.

TABLE 3.1. IMAGE PROCESSING FACILITY PARAMETERS

Effective Read Aperture Size & Shape	-	Circular 0.003 inch
Read Line Advance	-	0.001 inch
A/D Conversion Along Scan	-	33 K sample/second
Quantization	-	9 bits
Effective Write Aperture Size & Shape	-	Square 0.003 inch
Read and Write Spot Rate	-	80 ips
Input/Output Scale Factor	-	1:1

The circular read aperture was adjusted to 0.003 inch diameter which resulted in an effective spot size of 0.138 nmi diameter on the ERTS 70mm negatives. The output of the read detector was digitized to 9-bit accuracy at a 33K sample/sec rate along each scan line. Perpendicular to scan direction the line advance of the scanner is 0.001 inch. Thus it was only necessary to process every third line, i.e., just contiguous lines in the computer. The other two lines were discarded. The theoretical Modulation Transfer Function (MTF) for the read aperture is shown in Figure 3.2. This represents the MTF in the direction perpendicular to the scan where the effective sampling rate is $2Xf_o$. (f_o is defined in this report to be that spatial frequency arising from two just contiguous apertures.) In the along scan direction, the 33K samples/sec operating rate of the D/A converter is equivalent to $2.5Xf_o$ rate, resulting in a slightly higher MTF in that direction. Also shown in Figure 3.2 is experimental verification of the MTF. The driving function of the aperture was a squarewave, and the data points compare favorably to the squarewave response of a 0.003-inch diameter circular aperture.

Processing of the digital data stream in the computer was carried out maintaining the 9-bit accuracy. Truncation of the least significant bit was accomplished just before output from the computer. Thus, 8-bit words were routed to a zero order hold in series with a D/A converter. The output of the converter was used to drive the write aperture of the scanner. Although the focused aperture of the scanner itself is a 0.001 inch square, identical depositions of this aperture for three lines (3X0.001" = 0.003") and a deposition every 0.0024 inch along the line produces an effective output aperture of approximately a 0.003-inch square. The theoretical MTF for a 0.003-inch square aperture along with experimental points produced from using a squarewave driving function are shown in Figure 3.2.

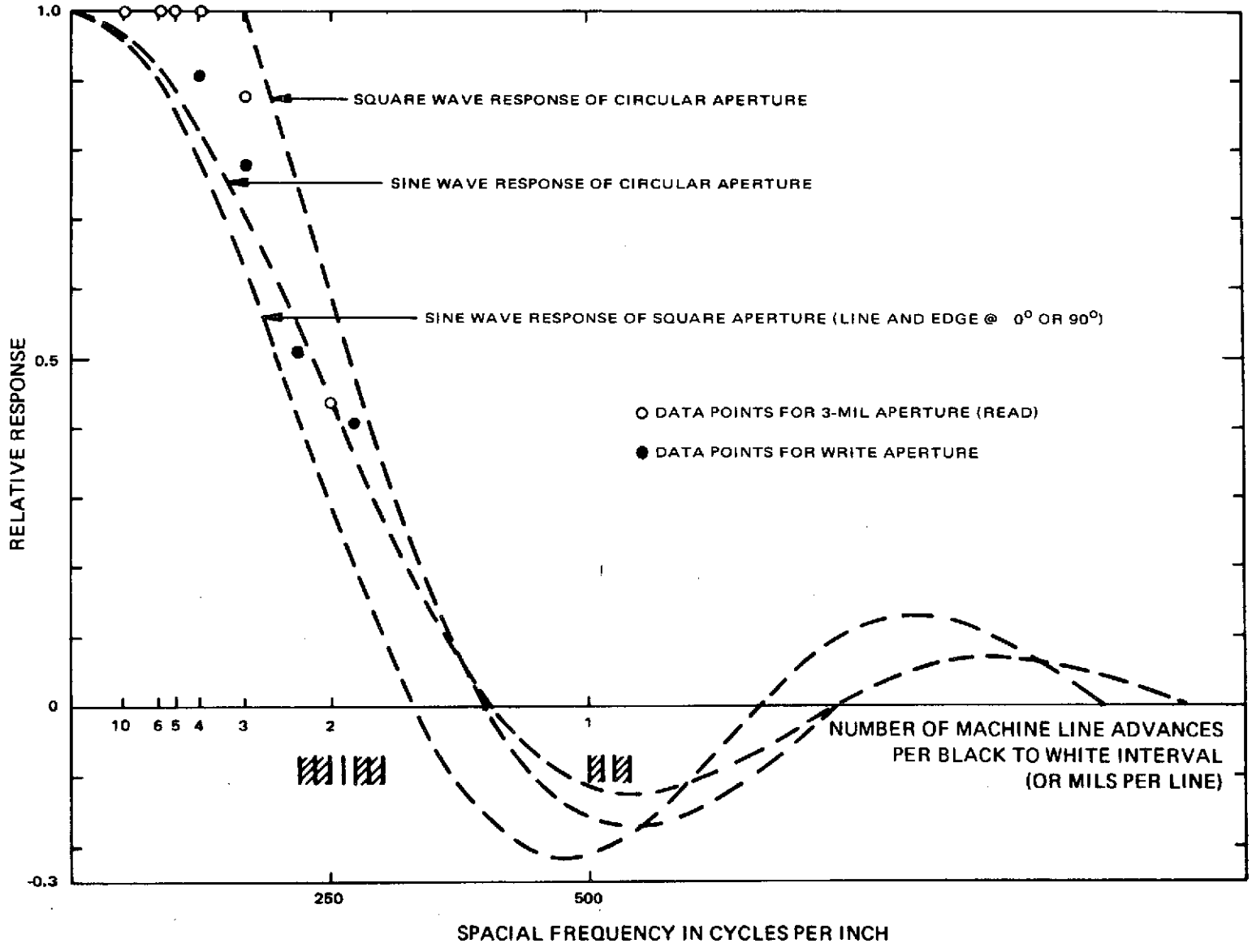

Figure 3.2. Read and Write Aperture Modulation Transfer Functions (MTF's)

3.1.2 Photographic Parameters

The photographic transfer characteristics of the scanner from input transparency to output transparency are controllable. However, limitations on this experiment were imposed by the standard operating configuration of the facility. The parameters controlling the output density could not readily be changed since the facility was also being used for other programs during the time period in which this experiment was conducted. The color scanner/computer processing system was calibrated in a configuration to produce output negatives in a density range of from 0.2 to 1.8. This resulted in a loss of information at densities in the ERTS negatives of from 0.4 to 0.7, or the lowest 2.0 percent of the sensor's output range. This was considered a satisfactory approach in light of the difficulty that would be encountered in changing the configuration of the facility and re-calibrating before and after each processing run. Furthermore, high albedo areas in the scene (high densities in the negative) were of prime interest and these were unaffected. Also, the contrast resulting from this process would more closely approximate those in a normal meteorological image, where a dynamic range greater than that of the MSS is required. Figure 3.3 is a sample calibration showing the typical in/out relationship for the resolution reduction process.

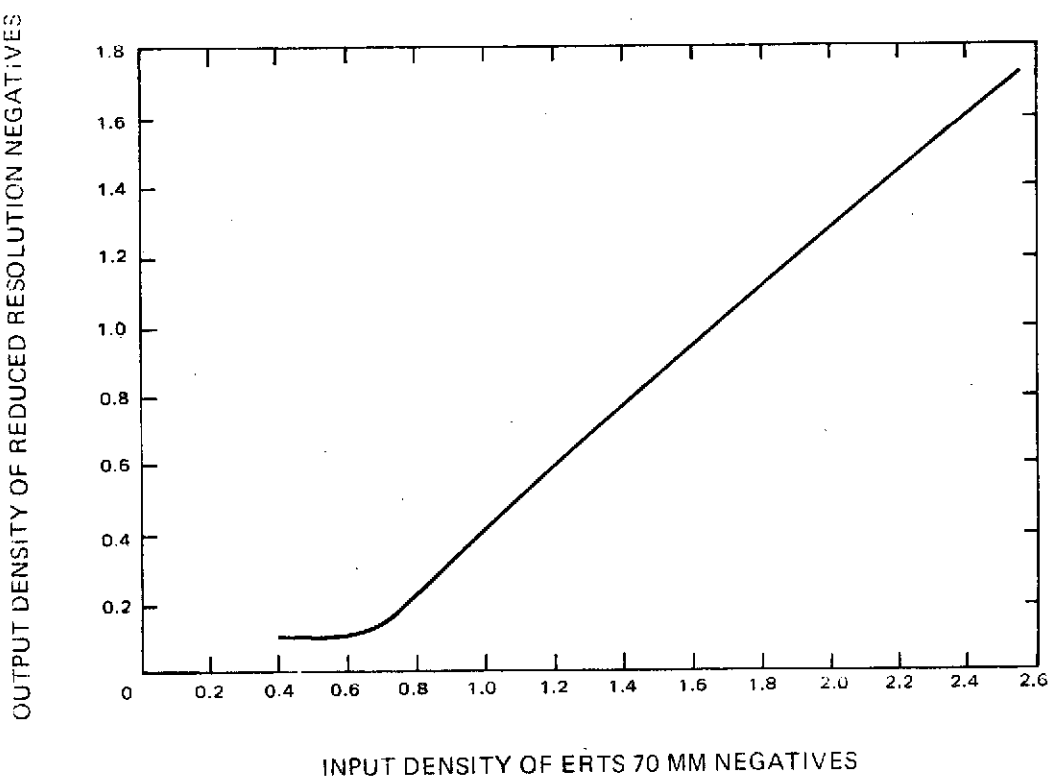

Figure 3.3. Density Transfer Characteristic of the Color Scanner

During the course of the study, reduced resolution negatives were produced on two different films. Originally Lumiere Lumilth film was used but after the supply was exhausted, additional film could not be readily obtained. Consequently, Kodak 2496 film was used for subsequent processing. Both were more than adequate in terms of spatial frequency response.

3.1.3 Processing Algorithms

As was originally proposed, the reduced resolution imagery produced by this experiment were simulations of data acquired by scanning radiometers with effective IFOV's of 1/8, 1/4, and 1/2 nmi. The limiting resolution of the degraded data was actually greater than the element size, as it would be in actual data acquired from radiometers. This approach to the experiment was adopted in order to make the results directly relatable to sensor design parameters. On the other hand, the effective resolution is reduced by aliasing. This factor is discussed in Section 3.1.4.

The general processing scheme is shown in Figure 3.1. The 1/8 nmi imagery was produced by a direct input/output process through the color scanner, while the production of the 1/4 and 1/2 nmi data required use of digital filtering techniques in the computer.

3.1.3.1 One-Eighth Nautical Mile Simulation

The 0.003-inch diameter color scanner aperture was used for two reasons. First, the scale of the ERTS 70mm format is such that this aperture size will produce an effective resolution element size of 0.1385 nmi in the along track direction, or approximately the 1/8 nmi desired for the experiment. Also, this aperture size is approximately the resolution of the unaided eye at 10 inches. Thus the output imagery would not need enlargement in order to perform a visual analysis of the imagery. The degradation process performed by the color scanner is depicted in Figure 3.4. The ERTS 70mm negative is read by the scanner, digitized, converted back to analog, and an output negative produced.

The scanner simulates a scanning radiometer acquiring data with an effective resolution element size of 0.138 nmi. The theoretical MTF of the data produced by this process in the direction perpendicular to the scan is shown in Figure 3.6. As can be seen, the process reproduces spatial frequencies higher than f_o with a significant response. The limiting resolution for this imagery is approximately 0.09 nmi.

3.1.3.2 One-Fourth Nautical Mile Simulation

The simulation of a scanning radiometer with an effective element size of 1/4 nmi was accomplished by performing a 2X2 element average on the samples produced after reading the 70mm ERTS negatives on the color scanner. This averaging process, accomplished in the computer, is depicted in Figure 3.4. The averaging process was accomplished contiguously in both orthogonal directions yielding approximately an 0.006-inch square aperture and an

I DIRECT IN/OUT

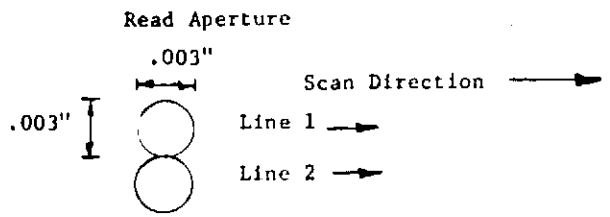

Sampling rate perpendicular to scan line = 2 x f_o where f_o is aperture frequency.

Digital samples taken every 2.4 mils along line (2.5 x f_o)

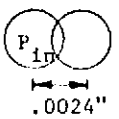

Effective aperture $\simeq$ .003" $\approx$ 0.138nmi

$$P_{in} = P_{out}$$

II Average 2; shift 2 (both along and across scan)

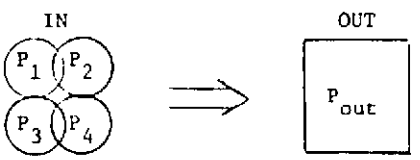

Effective aperture $\simeq$ .006" square

$$P_{out} = P_1 + \frac{P_2 + P_3}{4} + P_4$$

III Average 4; shift 4 (both along and across scan)

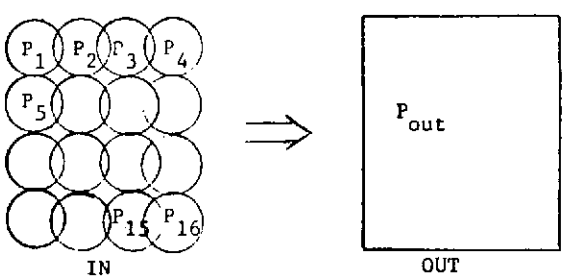

Effective aperture $\simeq$ 0.12" square

$$P_{out} = P_1 + \frac{P_2 + \cdots + P_{15}}{16} + P_{16}$$

Figure 3.4. Resolution Reduction Algorithms

effective sampling rate of $2Xf_o$. The samples were displayed as 0.006-inch squares. This was accomplished by the deposition of 36 identical values by the write aperture of the scanner.

Figure 3.5 shows the theoretical MTF of the 2X2 digital filtering process. The output MTF of the 1/4 nmi imagery is shown in Figure 3.6. This results from a serial combination of the read aperture MTF, the 2X2 read process MTF, the 2X2 write process MTF, and the write aperture MTF. Again, there is significant response at spatial frequencies higher than f_o. The limiting resolution for data produced by this process is less than 0.2 nmi.

3.1.3.3 One-Half Nautical Mile Simulation

An effective resolution element size of 1/2 nmi was produced by performing a 4X4 average process on the directly read digital samples. This results in an effective aperture of 0.012 inch square. The process is depicted in Figure 3.4.

During Phase I of the study, after all of the processes were developed and simulations were run on Gemini photographs, a phenomena which will be called "spatial contour noise" in this report was observed. It is well known that if square picture elements are displayed of such size that their element boundaries are easily discernible, the pattern recognition process is degraded. The 4X4 average process run on the Gemini images exhibited this contour noise. This is shown in Figure 3.7a. The effect can be eliminated by viewing the image at a reduced scale or at an increased distance such that the aperture size is just at or below the resolution of the eye. Alternatively, the output aperture shape can be "smoothed" such that the sharp contours are no longer apparent. This latter approach of output interpolation was adopted for the 1/2 nmi process. The two-dimensional, linear interpolation process used is shown in Figure 3.8 and the resulting effect on the imagery is shown in Figure 3.7b. This same effect is observable to a lesser degree in the 2X2 average process. However, for the 2X2 process it was not sufficiently objectionable to require interpolation.

The theoretical MTF for the 4X4 average process with and without output interpolation is shown in Figure 3.5. The MTF of the imagery resulting from the simulation of the 1/2 nmi scanning radiometer is shown in Figure 3.6 and was obtained by the serial combination of the write aperture MTF, the 4X4 average read MTF, the interpolation write MTF, and the write aperture MTF. Here again, the limiting resolution of the imagery is greater than f_o.

3.1.3.4 One Nautical Mile Simulation

Although not originally proposed as part of this experiment, attempts were made to produce simulations of a scanning radiometer with an effective aperture of 1 nmi. Two approaches were tried; however, because of the narrow coverage of the MSS swath (100 nmi) combined with the poor resolution, the data was difficult to interpret.

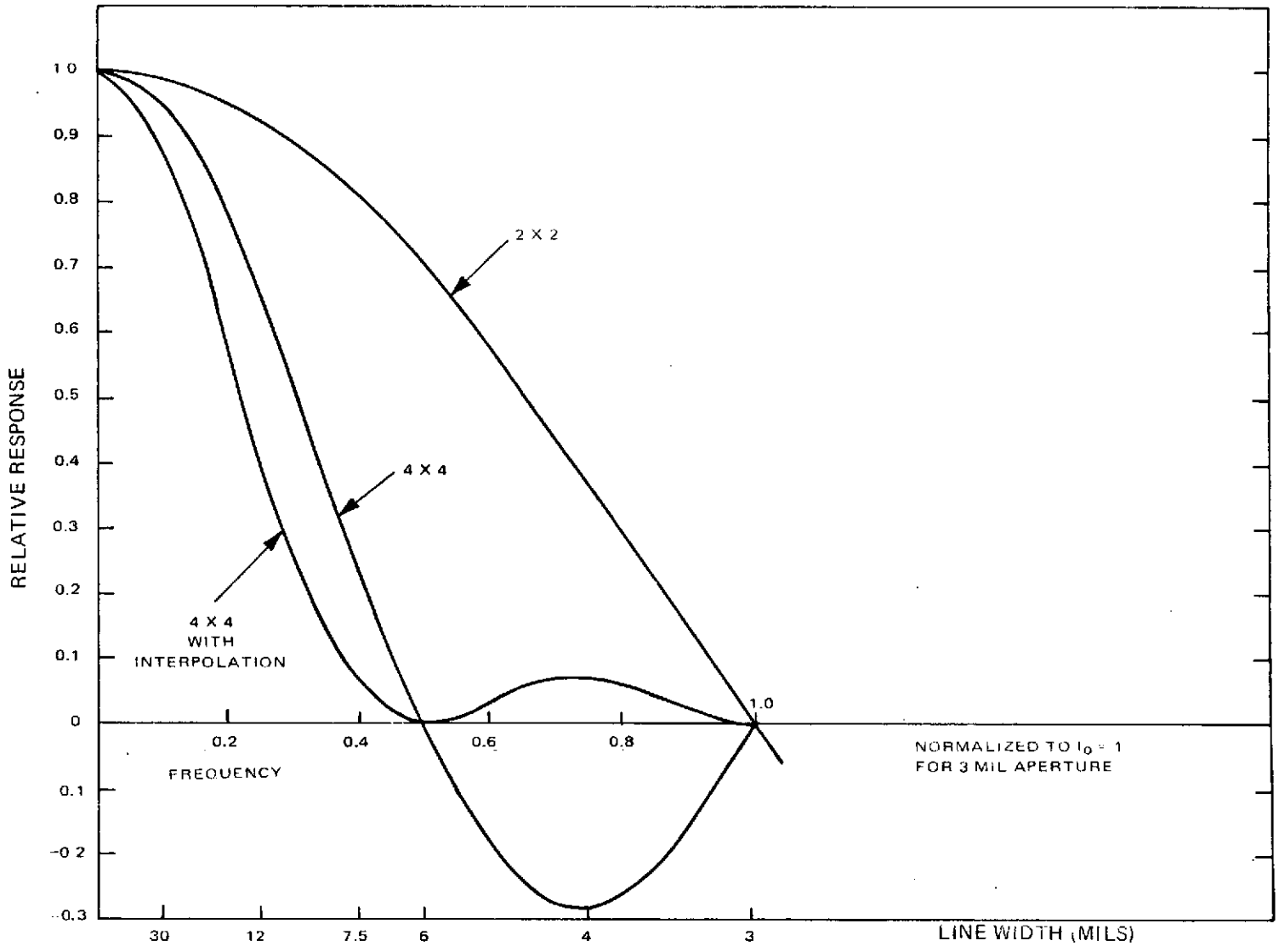

Figure 3.5. Processing MTF's Theoretical Sine Wave Response on Axis

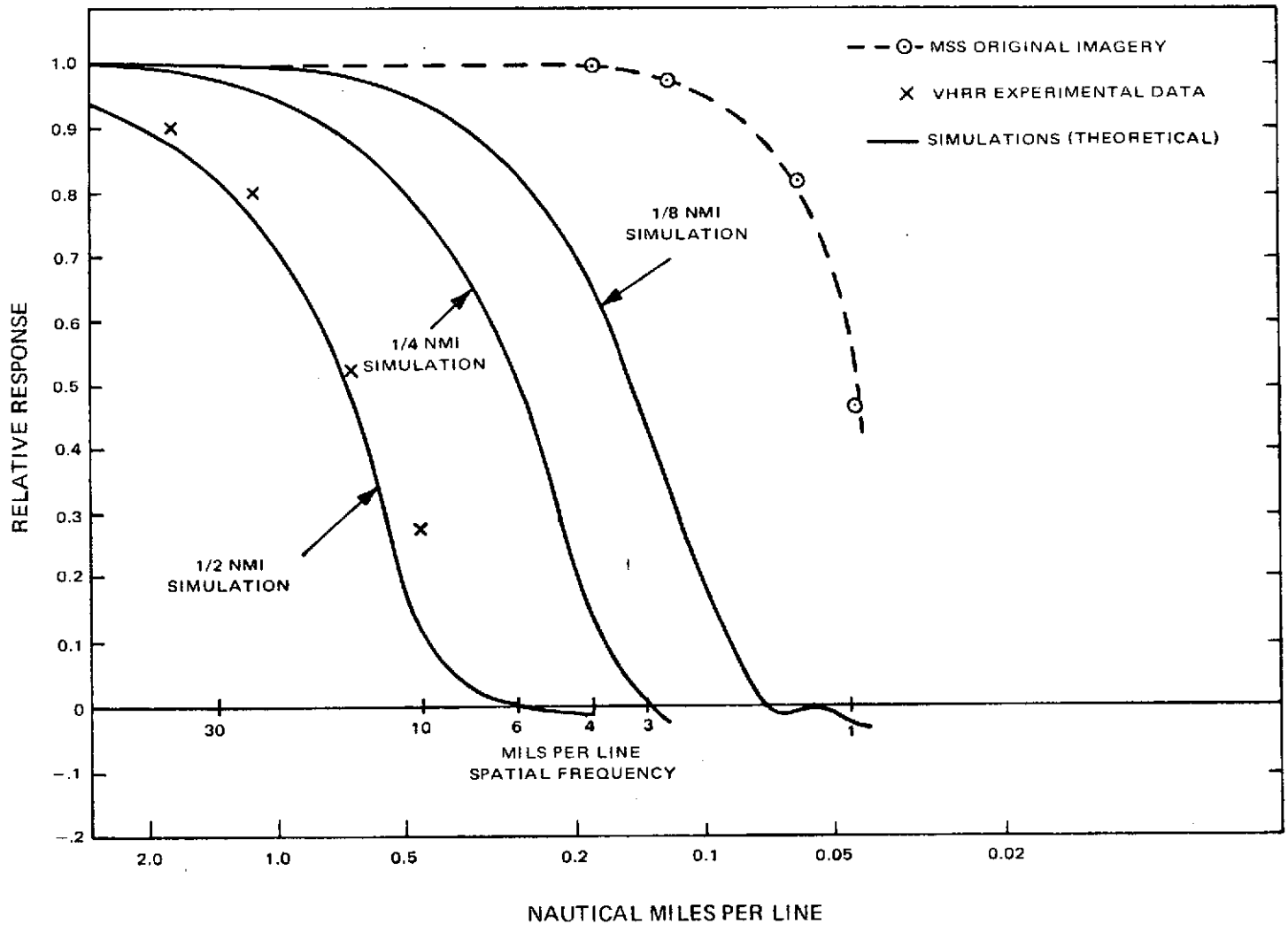

Figure 3.6 MTF of Reduced Resolution Output Imagery

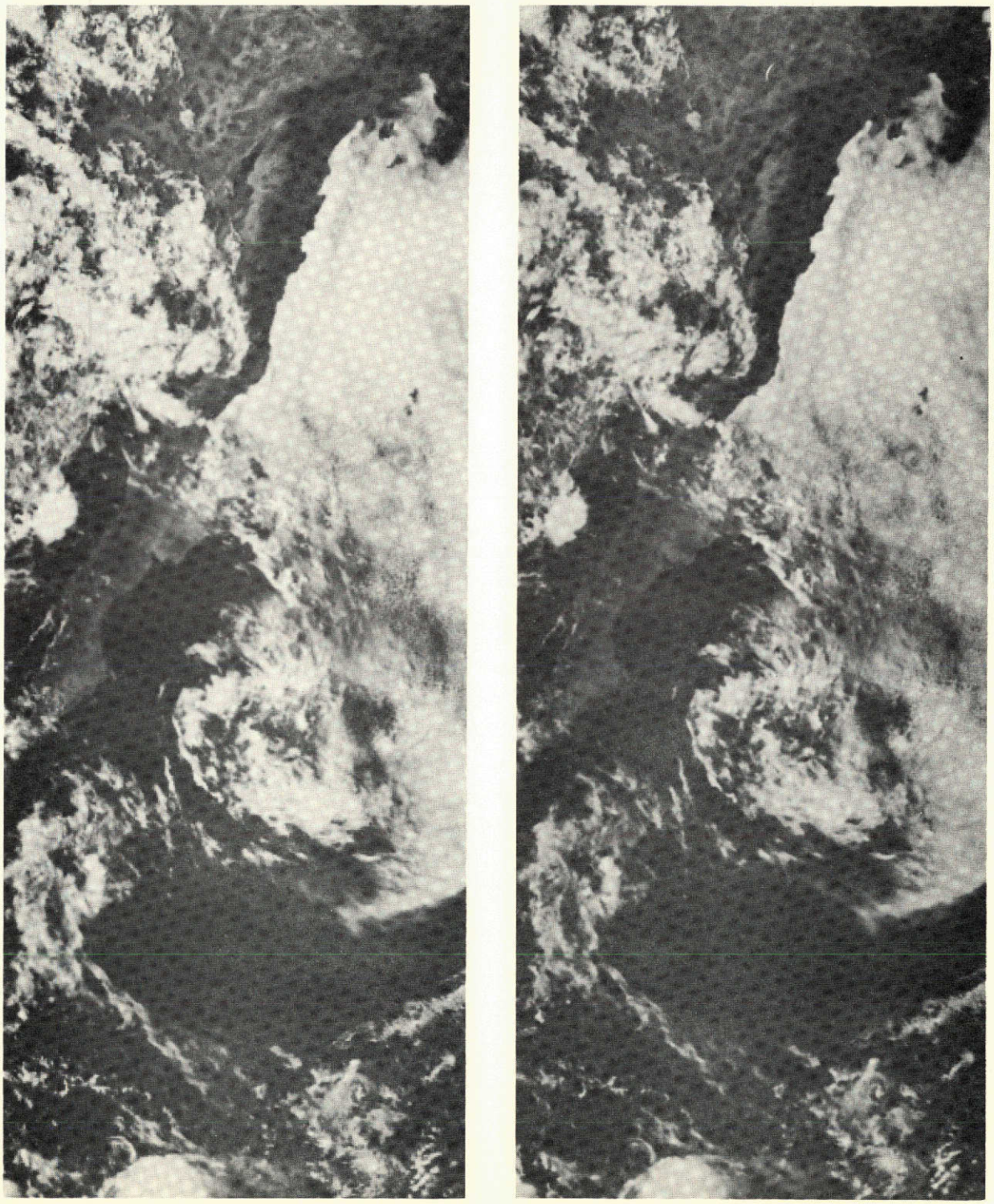

a. 4X4 Average
Without Interpolation

b. 4X4 Average
With Interpolation

Figure 3.7. Simulation of 4X4 Average Process

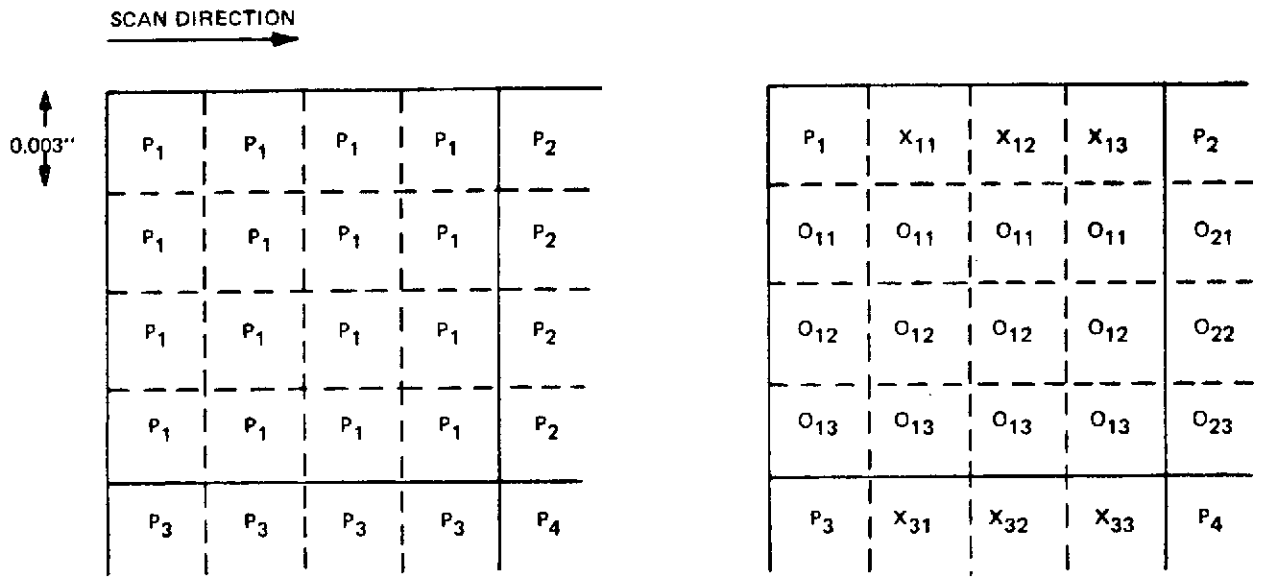

P_m = ORIGINAL PIXEL VALUE AFTER AVERAGING

X_{mm} = PIXEL VALUE AFTER LINE INTERPOLATION

O = PIXEL VALUE AFTER ROW INTERPOLATION

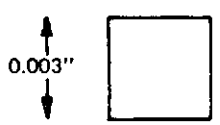

= "READ" PIXEL SIZE

INTERPOLATION ALGORITHM – 4 X 4 AVERAGE

$P_m = P_m$

$X_{m1} = 3/4\ P_m + 1/4\ P_{m+1}$

$X_{m2} = 1/2\ P_m + 1/2\ P_{m+1}$

$X_{m3} = 1/4\ P_m + 3/4\ P_{m+1}$

$O_{m1} = 3/4\ P_m + 1/4\ P_{m+1}$
OR
$3/4\ X_{mn} + 1/4\ X_{m+1\,n}$

$O_{m2} = 1/2\ P_m + 1/2\ X_{m+1\,m}$
OR
$1/2\ X_{mn} + 1/2\ X_{m+1\,n}$

$O_{m3} = 1/4\ P_m + 3/4\ P_{m+1}$
OR
$1/4\ X_{mn} + 3/4\ X_{m+1\,n}$

Figure 3.8. Interpolation Process

For three scenes, the output of the 1/2 nmi simulation was reduced to 1/2 the original size and processed again on the scanner using the 1/4 nmi process. This resulted in a simulation of a 1-nmi aperture size.

Also, an 8X8 average process was run on the original ERTS negatives for three scenes. Output interpolation could not be used because of memory limitations on the computer. The resulting simulation of 1 nmi aperture exhibited severe contour noise.

As a result of these attempts, it was concluded that satisfactory results could not be obtained with this combination of resolution and field-of-view.

3.1.3.5 Aliasing

Aliasing will occur in the degraded images as a result of the effective sampling rate of the algorithms being at or just above the Nyquist rate. Aliasing occurs when a particular spatial frequency is erroneously displayed as a lower spatial frequency. This introduction of erroneous information occurs for spatial frequencies higher than f_o. An example of these phenomena can be seen in the resolution charts at the top of Figure 3.7. Here only high spatial frequencies are present and the aliasing, which shows up as cross banding in the bar targets, is clearly visible. In a typical scene with a wide variety of spatial frequencies aliasing is not readily apparent and the interpretability of the imagery will be generally unaffected at frequencies lower than f_o. However, the aliased energy can be thought of as a type of noise in the image. This general point is brought up only for the sake of completeness. The aliasing in these simulations, while slightly more than would be anticipated in a correctly designed radiometer system, is small enough to have a negligible effect on the visual interpretation of the imagery.

3.2 Results

During the resolution reduction portion of the experiment, twenty-five scenes were processed. The three reduced resolution scenes plus the original resolution scene are presented in 70mm format in Appendix A. These represent 6th generation products (three additional generations during the production of this report), and since elaborate photographic processes were not used to produce the copies for this report, variations in contrast exist in these copies. However, the analyses performed on each scene was accomplished using contact prints and transparencies made from the original output of the degradation process (4th generation product). Density range and gamma for these products were controlled.

When viewing the data in Appendix A, it is recommended that the 1/2 nmi simulation for each scene be examined first, with the others following in order of increasing resolution. This is suggested since the recognition threshold, once crossed, will involuntarily increase the amount of information that the observer feels he can see. Care was taken to analyze each scene processed in this experiment in order of increasing resolution.

While it is risky to draw conclusions from such a limited number of sample observations, the results of the analysis were very consistent in two areas:

(1) When using satellite acquired imagery in the 0.6 - 0.7μ band to determine cloud type, especially in layered conditions, 1/2 nmi resolution data is not adequate. In the vast majority of the cases examined, the 1/4 nmi resolution data was sufficient for observations of cloud cover. Only in the case of cloud cover over mountain snow was additional information provided by the 1/8 nmi resolution data.

(2) For observations of ice and snow in the 0.6 - 0.7μ band, the resolution requirement appears to be very variable. Sea ice is generally identifiable and differentiable from clouds at 1/2 nmi resolution. Surface snow and lake ice are also generally identifiable at 1/2 nmi resolution. The only exceptions being when partial cloudiness exists over the scene. Then the added surface detail allows for discrimination of the ice and/or snow.

3.2.1 Frames 1098-15141 through-15150 (Figures A-1 and 3.9)

These three frames, shown in Figure 3.9, were taken over the extreme northern section of Quebec, Canada on October 29, 1972. The images cover the west-center portion of a well developed low pressure center. The surface chart for 10/29/1200Z is shown in Figure 3.10.

The only portion of the scene which is not at least partially cloud covered is the area near A. There are two distinct cloud layers. At B and C a very low broken stratus deck exists; while the area near D is covered by an overcast stratus deck with shadows indicating a height of approximately 6000 feet. The following significant observations can be made about the degraded data:

(1) The large wave structure in the higher deck is evident at all resolutions.

(2) The cloud detail necessary to distinguish the lower broken deck from the partially snow covered surface is not present in the 0.5 nmi data. It is present to a degree in the 0.25 nmi data.

(3) The small wave structure in the lower deck is still apparent in the 0.13 nmi data and is beginning to disappear in the 0.25 nmi data.

3.2.2 Frames 1100-15325 through-15343 (Figures A-2A and B; and Figures 3.13A & B)

These frames form a swath from Georgia/South Carolina through Florida to the Gulf of Mexico south of Tampa on October 31, 1972. The synoptic situation (Figure 3.11) showed a large high centered over SE Canada causing a low level flow ($\approx$ 10 kts) from the ENE across the Florida peninsula. A trough through eastern Texas to Arkansas was causing widespread cloudiness and precipitation through central and east central U.S. Cloudiness from the eastern edge of this system is seen in the northern-most frame. A VHRR picture (resolution

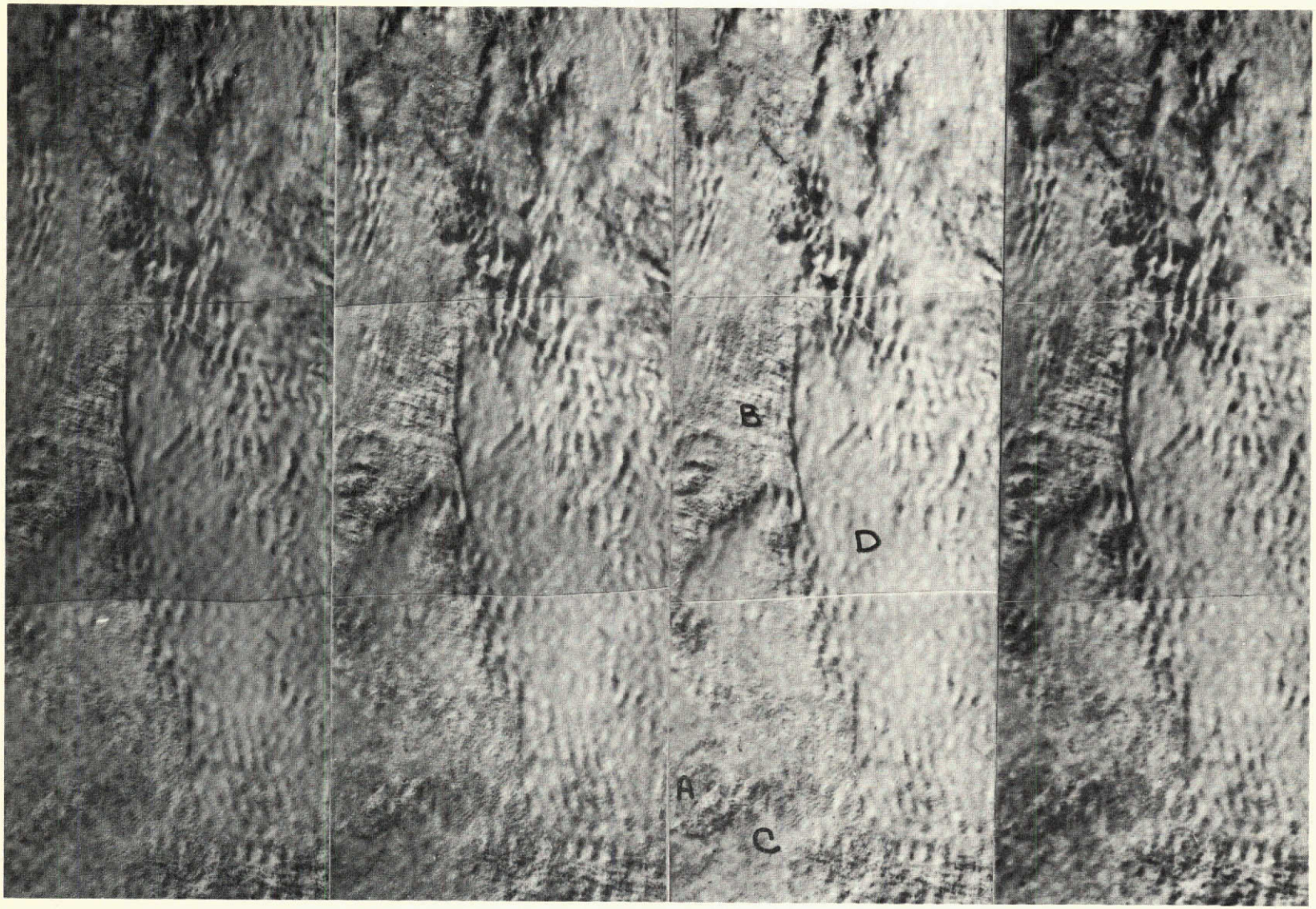

1/2 nmi. RESOLUTION | 1/4 nmi. RESOLUTION | 1/8 nmi. RESOLUTION | 100 METER RESOLUTION

Figure 3.9. Frames 1098-15141-15150

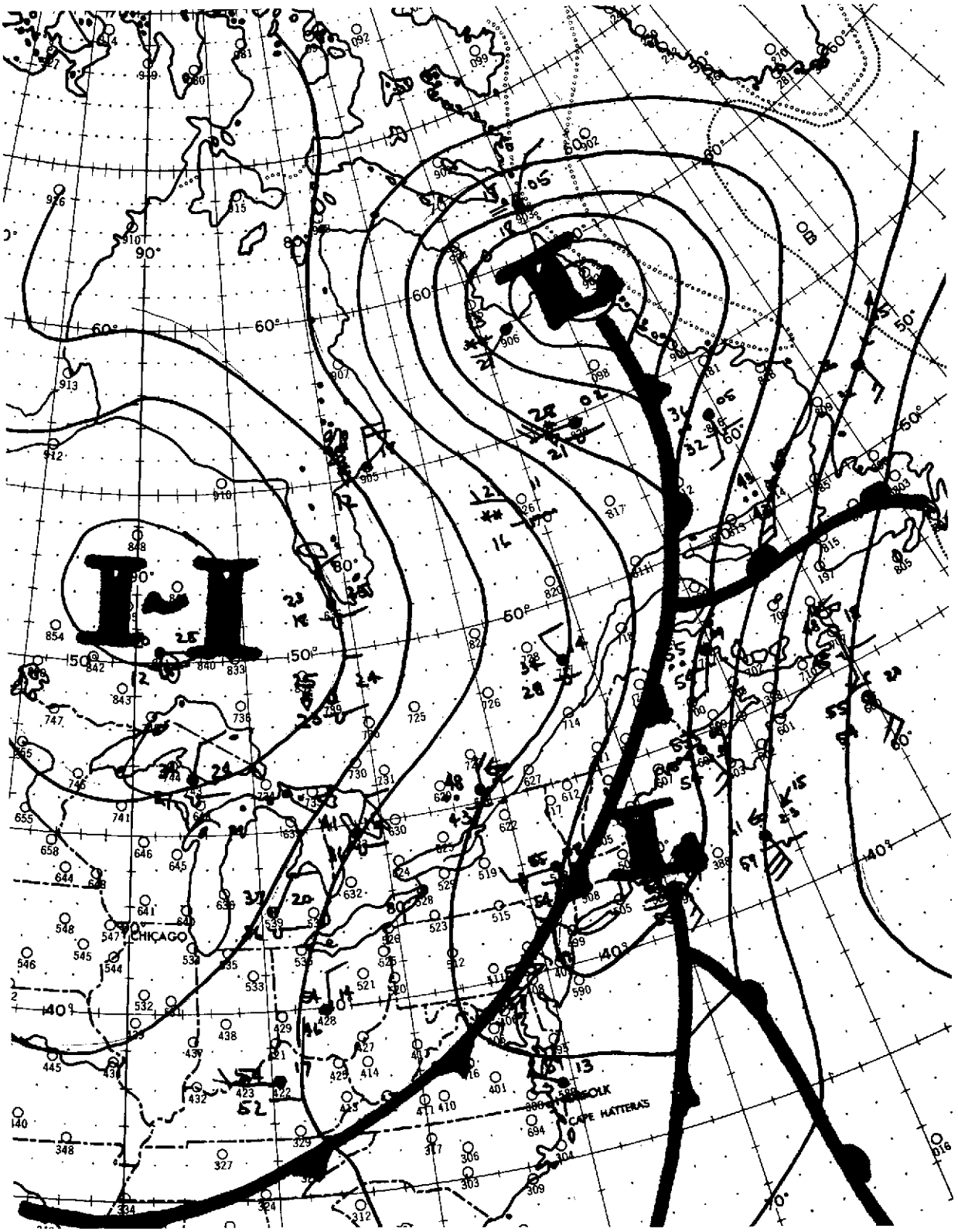

Figure 3.10. Surface Chart 10/29/1200Z

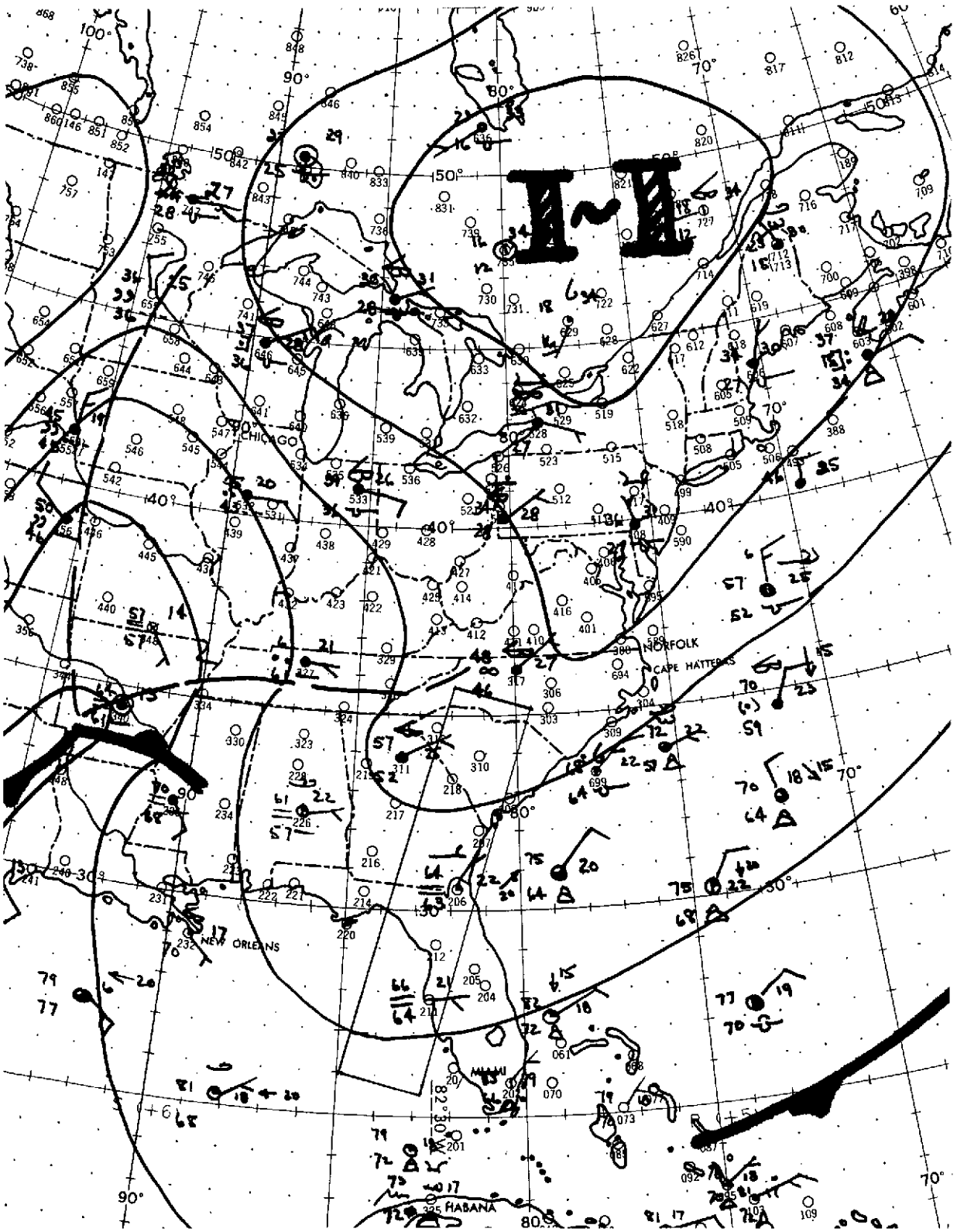

Figure 3.11. Spacecraft Chart 10/31/12Z

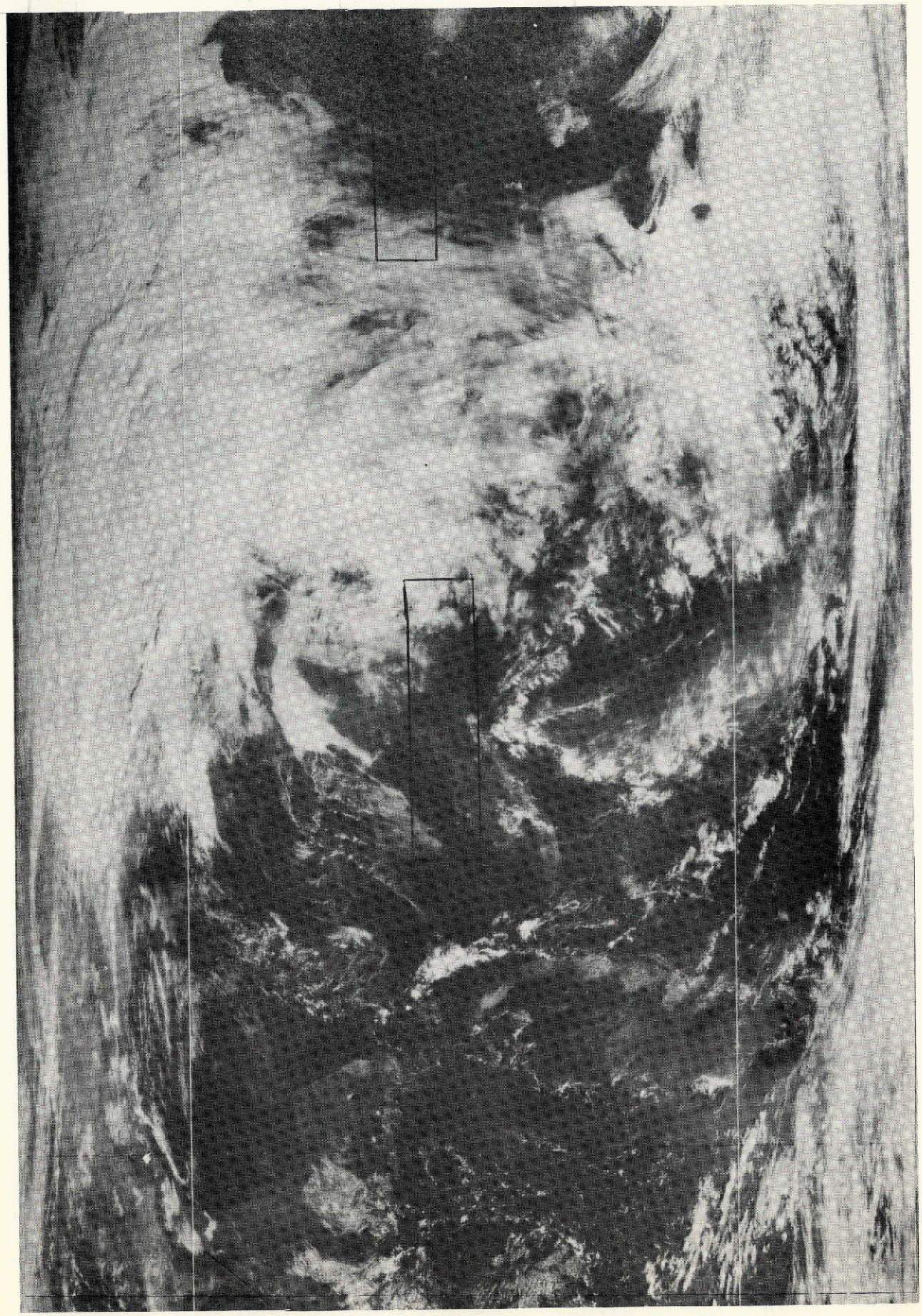

Figure 3.12. VHRR Image Oct. 31, 1972 (0.6 - 0.7μ)

0.5 nmi subpoint: 0.6μ - 0.7μ) from NOAA-2 is shown in Figure 3.12. This was taken about 40 minutes before the ERTS frames on the same day. The area covered by the ERTS frames is outlined. This photograph was made on the DRGS display made by Image Information, Inc., but through reproduction appears to have lost some of the original resolution. This fact is evidenced in Figure 3.13A and B where an enlargement of the VHRR photo is shown along with the corresponding degraded ERTS swath. Also note that the cumulus cloud field has developed rapidly during the 40-minute time interval between the pictures.

As for the degradation from 100 meter to 1/2 nmi resolution, little of the original meteorological information content is lost. The cumulus cloud streets (tops approximately 3,500 ft.) are still evident at 1/2 nmi although many of the smaller cells are lost. However, most of the wave structure, as well as the existence of several layers in the northern-most frame, has been lost in 1/2 nmi image but still clearly seen at 1/4 nmi.

The cirrus clouds west of Tampa (approximately 30,000 ft. altitude) remain identifiable in each of the degraded scenes.

3.2.3 Frames 1100-15284 through -15293 (Figures A-3 and 3.14)

These frames are from the same pass as was discussed in Section 3.2.2 taken over Canada just north of Lake Erie. This is very near the center of the high pressure area. The cloud structure appears to have changed considerably in the 40-minute interval between the VHRR picture in Figure 3.12 and the ERTS frames shown in Figure 3.14. Cirrus becoming cirrostratus in the southern-most frame predominates this scene. Middle level wave clouds can be seen in the center frame and an underlying deck of altocumulus begins near the bottom of the scene. In all the degraded pictures the main meteorological features remain evident, except for the fact that altocumulus near the bottom of the scene has lost much of its character in the 1/2 nmi image.

3.2.4 Frames 1099-17020 through 1099-17025 (Figures A-4 and 3.17)

These three frames were taken over the western edge of Hudson Bay on October 30, 1972. Figure 3.15 at X is the VHRR picture from NOAA-2 taken approximately 40 minutes before the ERTS data. There is a strong westerly low level flow (Figure 3.16) over the area. When the relatively cool air passes over the warm water, stratocumulus is formed over the bay. The new ice pack along the edge of the bay is clearly visible. Note the cyclonic nature of the flow over the bay. The resolution of the VHRR data at this point is approximately 0.75 nmi. Even at this resolution the ice with its radically different structure can be distinguished from the clouds.

The resolution degradation of the ERTS data (see Figure 3.17) does little to the meteorological information content of this scene. There appears to be low level fog or thin stratus along the west coast of the bay. Although still detectable at 1/2 nmi, most of its character has been lost. The stratus deck in the extreme southeast corner is still visible at 1/2 nmi as are the beginning of the cumulus streets at the eastern edge of the ice pack. The newer ice is distinguishable from the old ice because of its lower albedo.

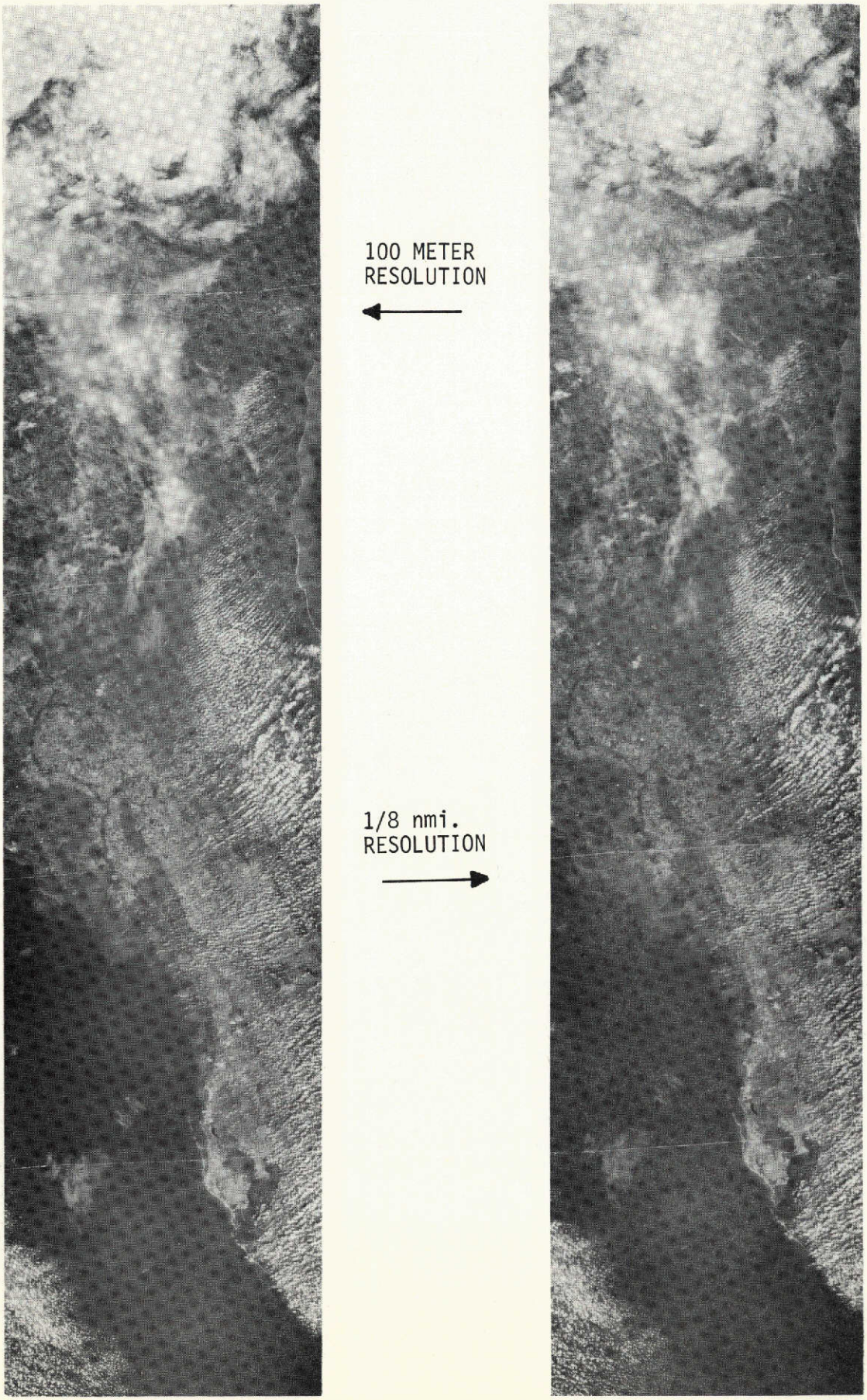

Figure 3.13a. Frames 1100-15325-15343

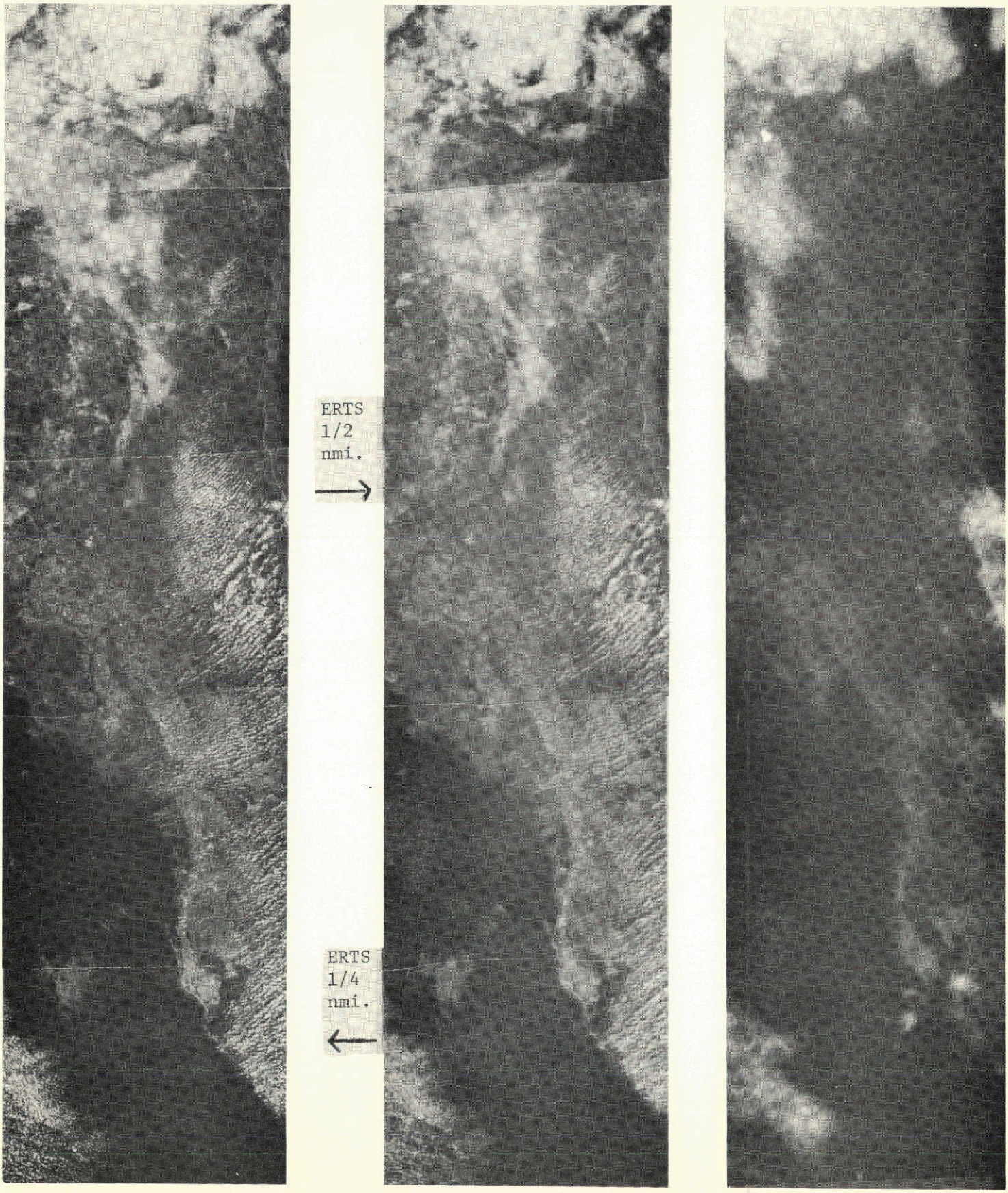

Figure 3.13b. VHRR Enlargement and Frames 1100-15325-15343

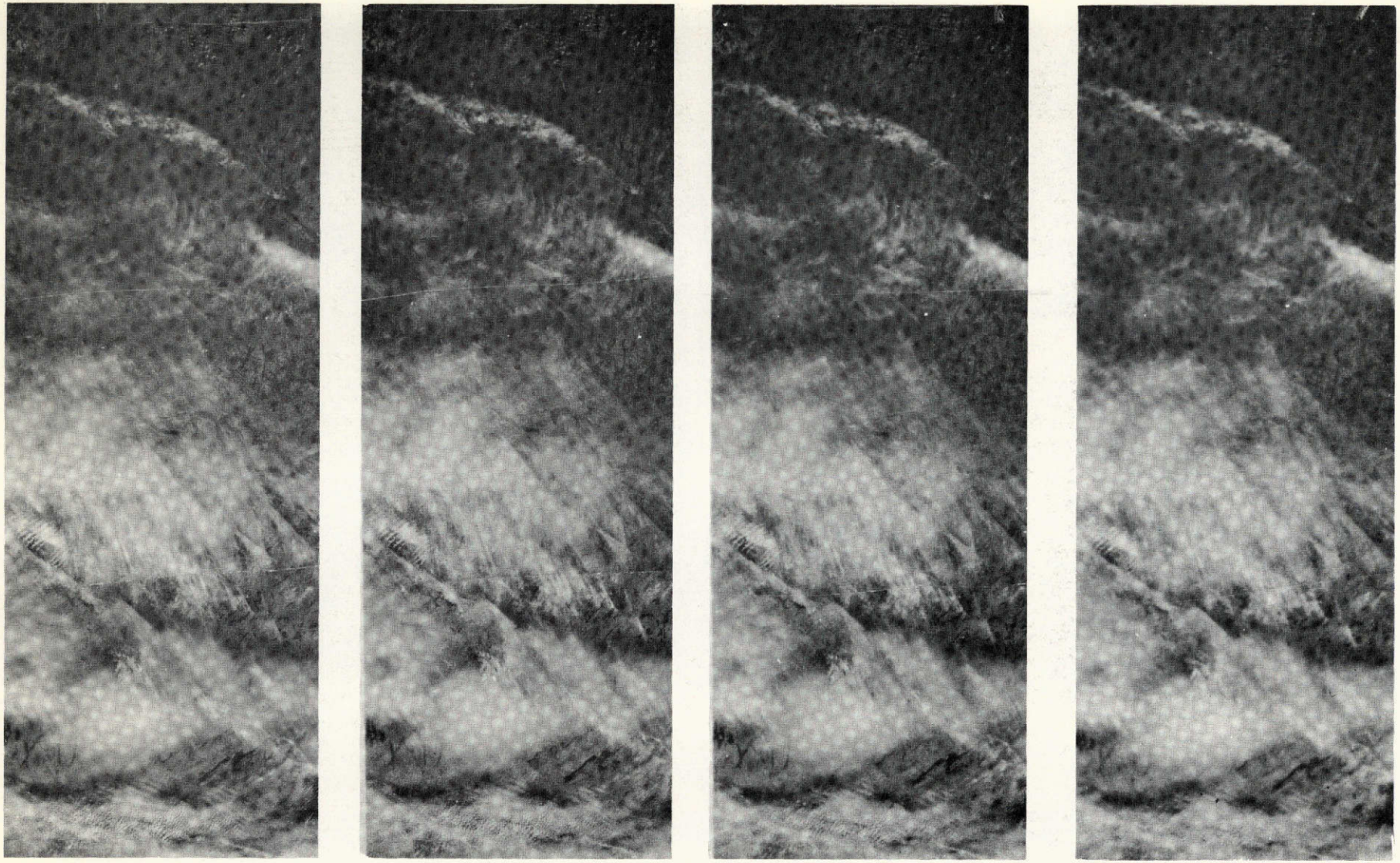

100 METER RESOLUTION

1/8 nmi. RESOLUTION

1/4 nmi. RESOLUTION

1/2 nmi. RESOLUTION

Figure 3.14. Frames 1100-15284-15293

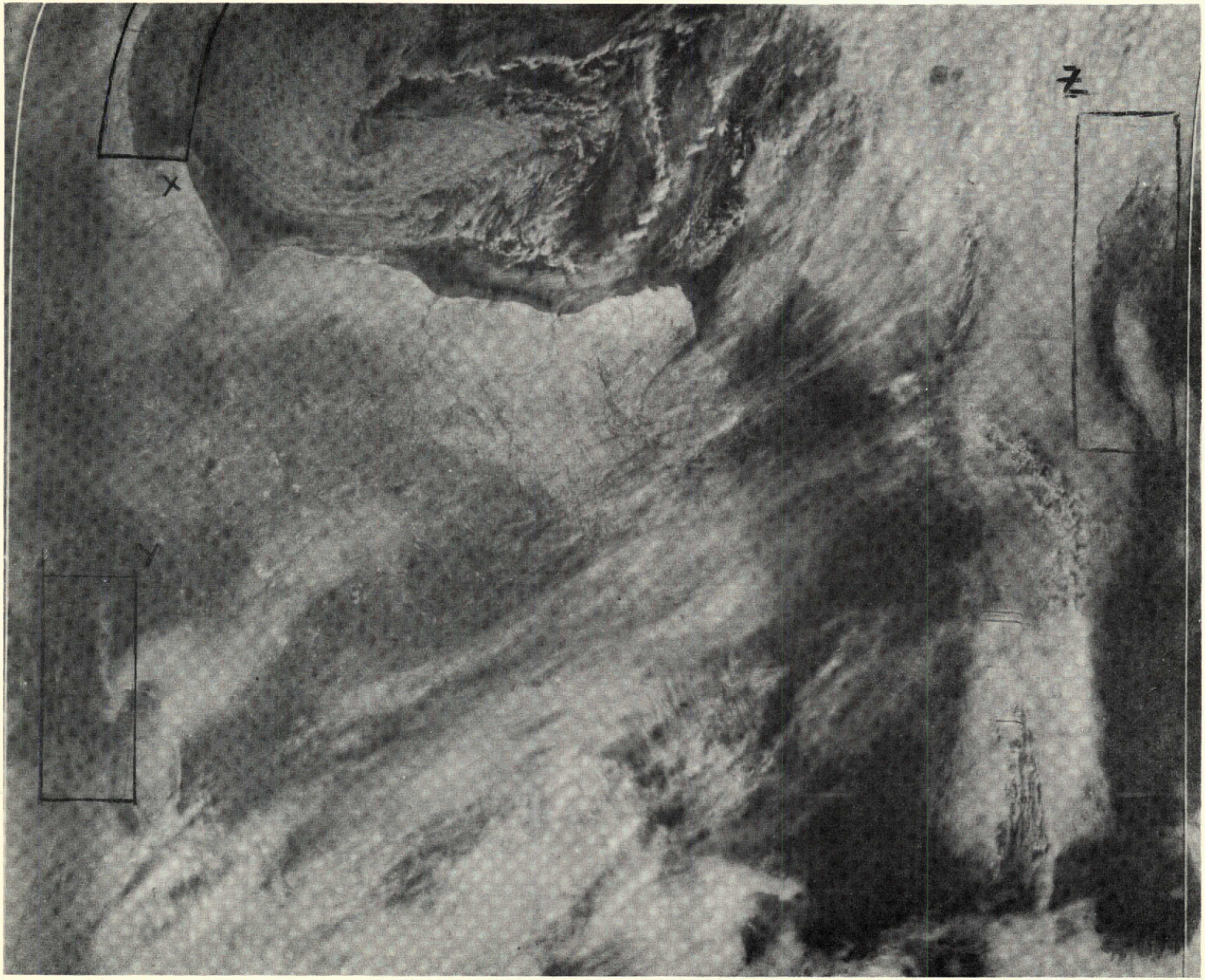

Figure 3.15 VHRR Image October 30, 1972 (0.6-0.7μ)

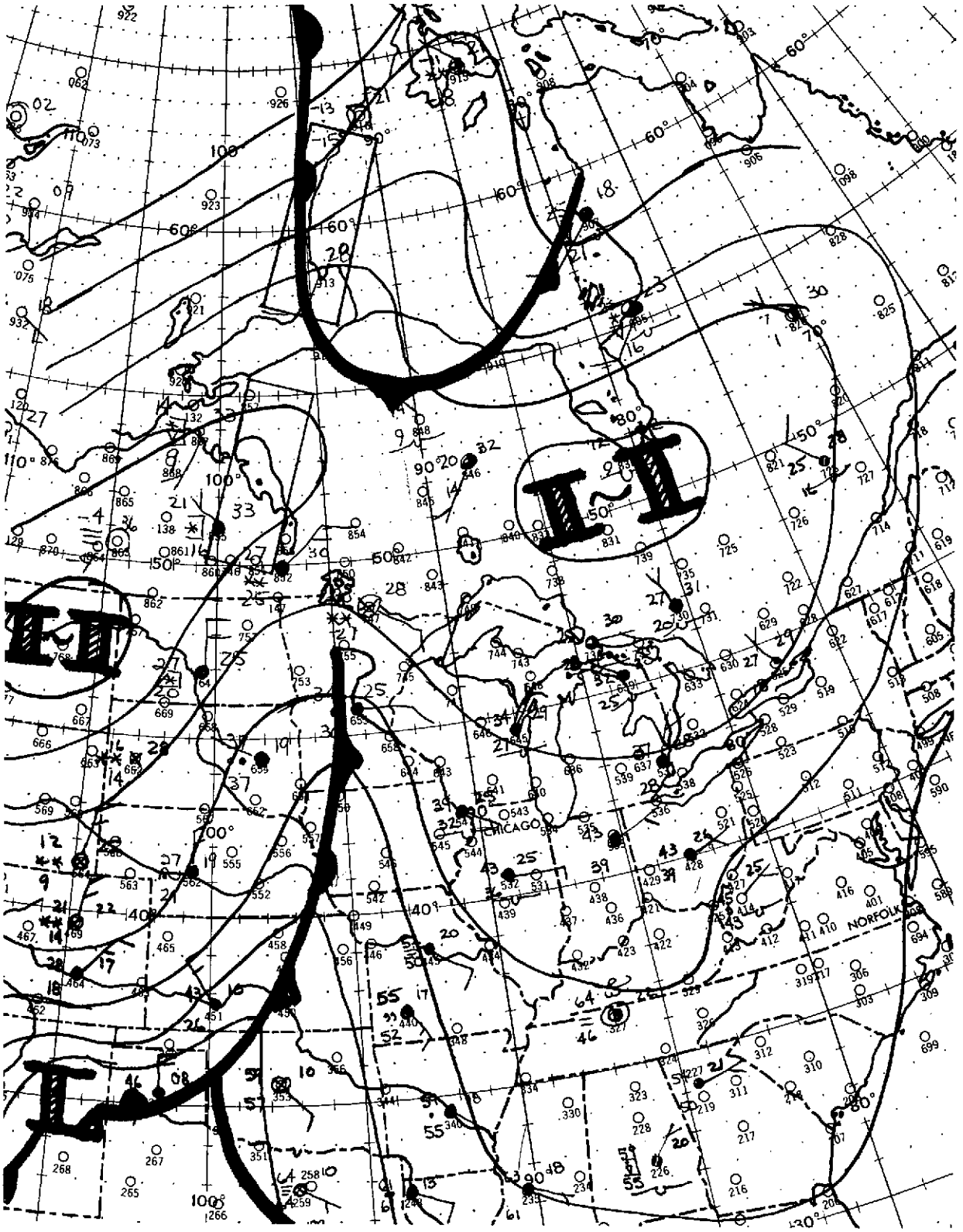

Figure 3.16 Surface Chart 10/30/1200Z

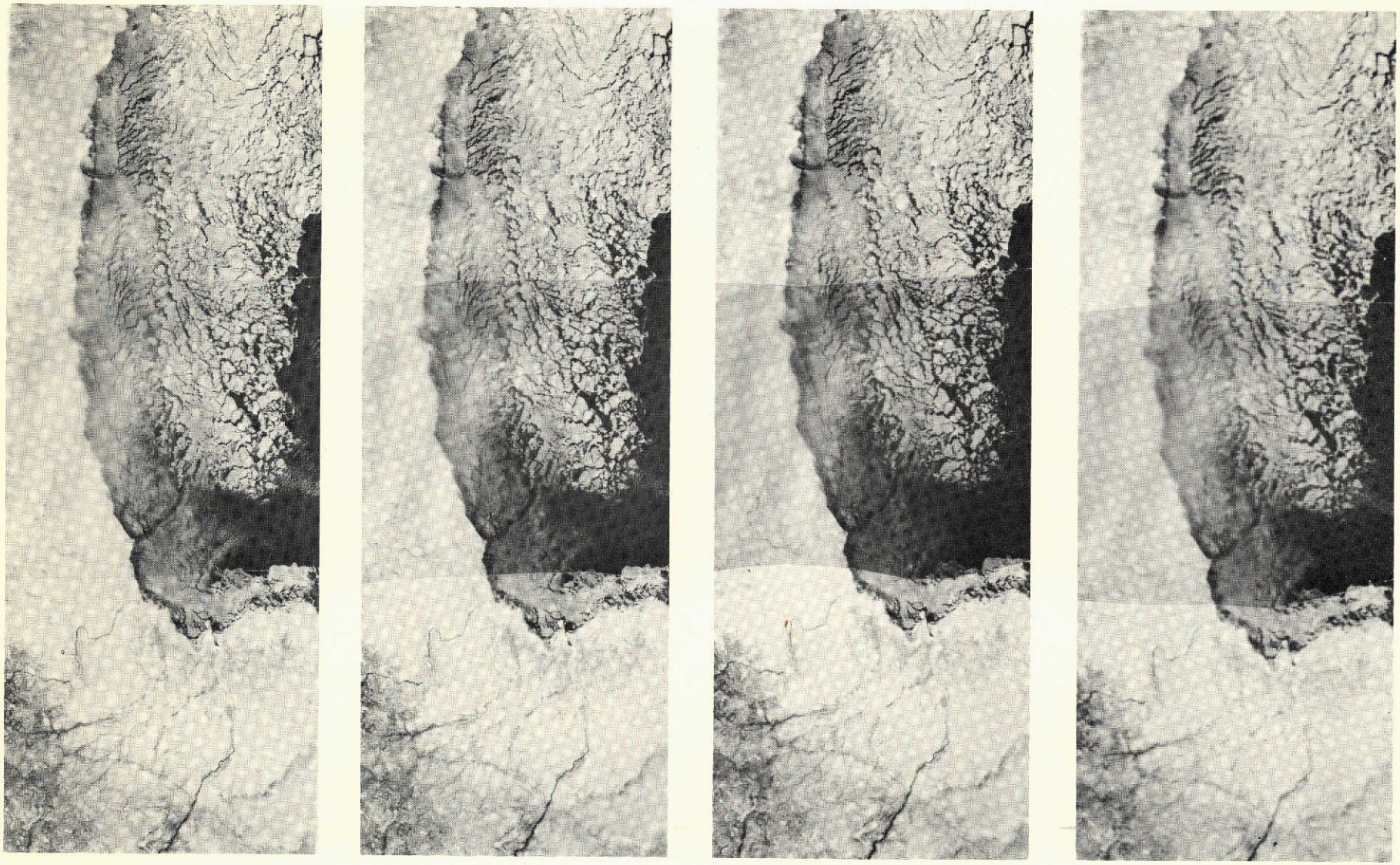

100 METER RESOLUTION

1/8 nmi. RESOLUTION

1/4 nmi. RESOLUTION

1/2 nmi. RESOLUTION

Figure 3.17 Frames 1099-17020-17025

3.2.5 Frames 1099-17040 through -17045 (Figures A-5 and 3.18)

This scene was taken during the same orbit as those in Section 3.2.4. This area is also outlined on the VHRR image (Y) in Figure 3.15. This synoptic situation is shown in Figure 3.16. The large area of general precipitation over the central U.S. begins at the bottom of this scene. Snow is occurring just to the southeast of the lowest frame. The new ice in the lake at A is clearly visible. The high albedo of the lake at B probably indicates new ice is forming. The stratocumulus over this lake is at about 3000 feet. The low overcast stratus deck at C ($\approx$ 1000 ft) is clearly visible against the snow background. Very small cumulus clouds at D and E are just beginning to form.

In the degraded images, shown in Figure 3.18, most elements of the scene are visible up through the 1/2 nmi resolution. The only things lost in the 1/2 nmi scene are the small cumulus fields at D and E and the ability to distinguish some clouds from ice and snow, for example, at F.

3.2.6 Frames 1121-17324, -17321 (Figures A-6 and 3.19)

The frames were taken on November 21, 1972, over southern Utah/northern Arizona. The ridges at B, C, and D are all snow covered. Many types of clouds are occurring in the scene. The wave stratocumulus clouds at A are approximately 2500 feet above the terrain. At C there appears to be thin altostratus or cirrostratus over the stratocumulus which is scattered in this area. There is also snow on the ground here. At E the cumulus is beginning to develop vertically. At B there are no apparent clouds over the snow covered ridge. At D underlying the thin clouds is an obvious dendritic snow pattern.

In the degraded photographs, information is rapidly lost. In the 1/2 nmi image, the only obvious fact remaining of those discussed above is the existence of the wave clouds at A. Even the dendritic pattern of the snow at B has disappeared. In the 1/4 nmi data, the only areas which would be difficult to interpret would be at D and C, and the vertical development at E. In 1/8 nmi data all of the situations pointed out are interpretable. Of course, at individual points in the pattern an erroneous cloud/snow decision might be made but the general situation is obvious.

3.2.7 Frames 1070-16034, -16041 (Figure A-7)

This scene covers the lower portion of Lake Michigan and Chicago on October 1, 1972. The synoptic situation showed a large high pressure system over the eastern U.S. with a trough and associated weak front lying NE-SW through northern Wisconsin. The low level flow over the area of the ERTS frame was from the southwest. The surface winds in the area were approximately 220^{0}/15 kts. and the 850 mb winds were approximately 260^{0}/20 kts.

A weak warm front was analyzed on the surface chart, NNW-SSE, approximately along the WSW edge of the formation of altocumulus clouds in the photograph. From shadow length, the cloud tops were calculated to be 9500 feet.

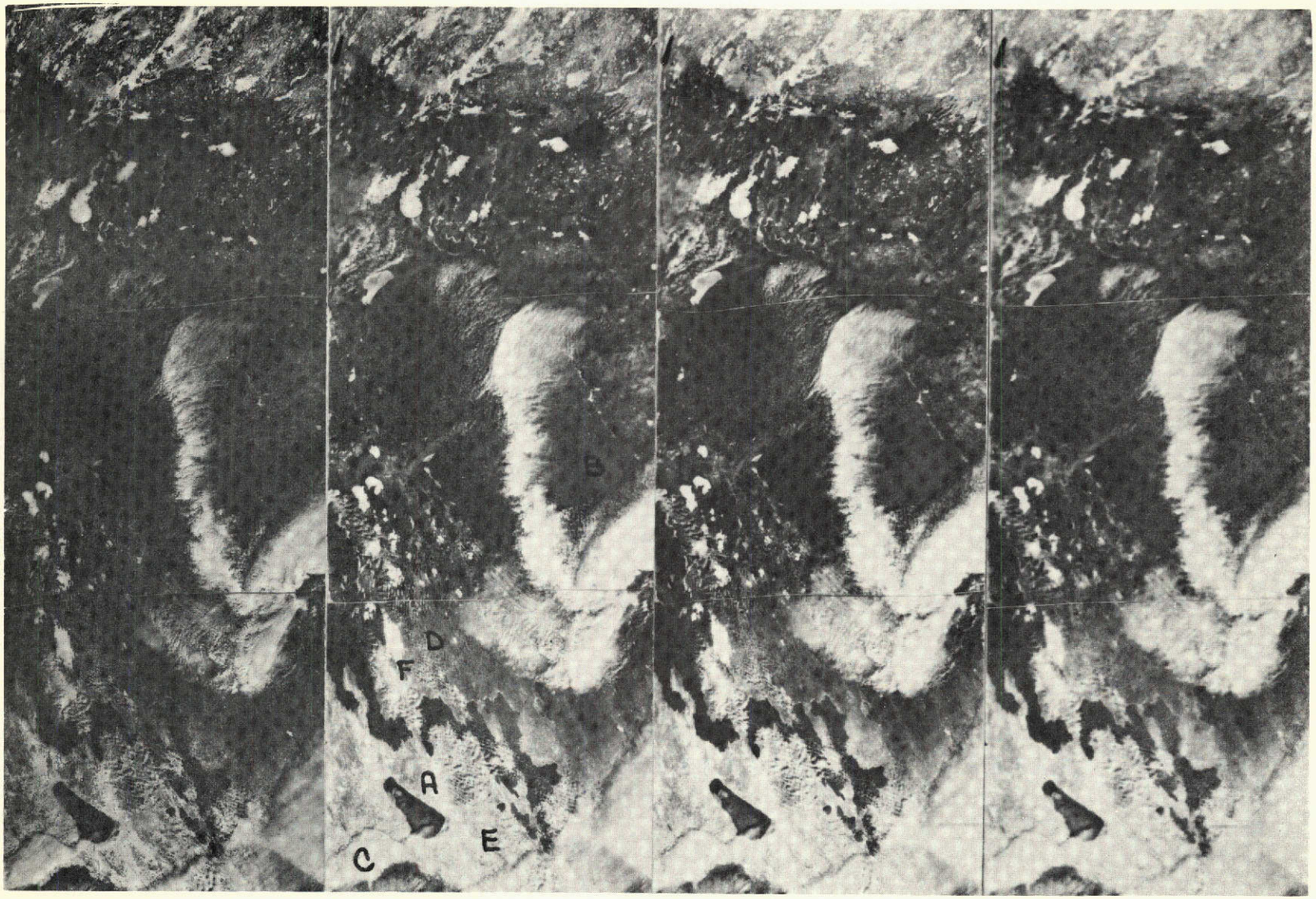

100 METER RESOLUTION | 1/8 nmi. RESOLUTION | 1/4 nmi. RESOLUTION | 1/2 nmi. RESOLUTION

Figure 3.18. Frames 1099-17040-17045

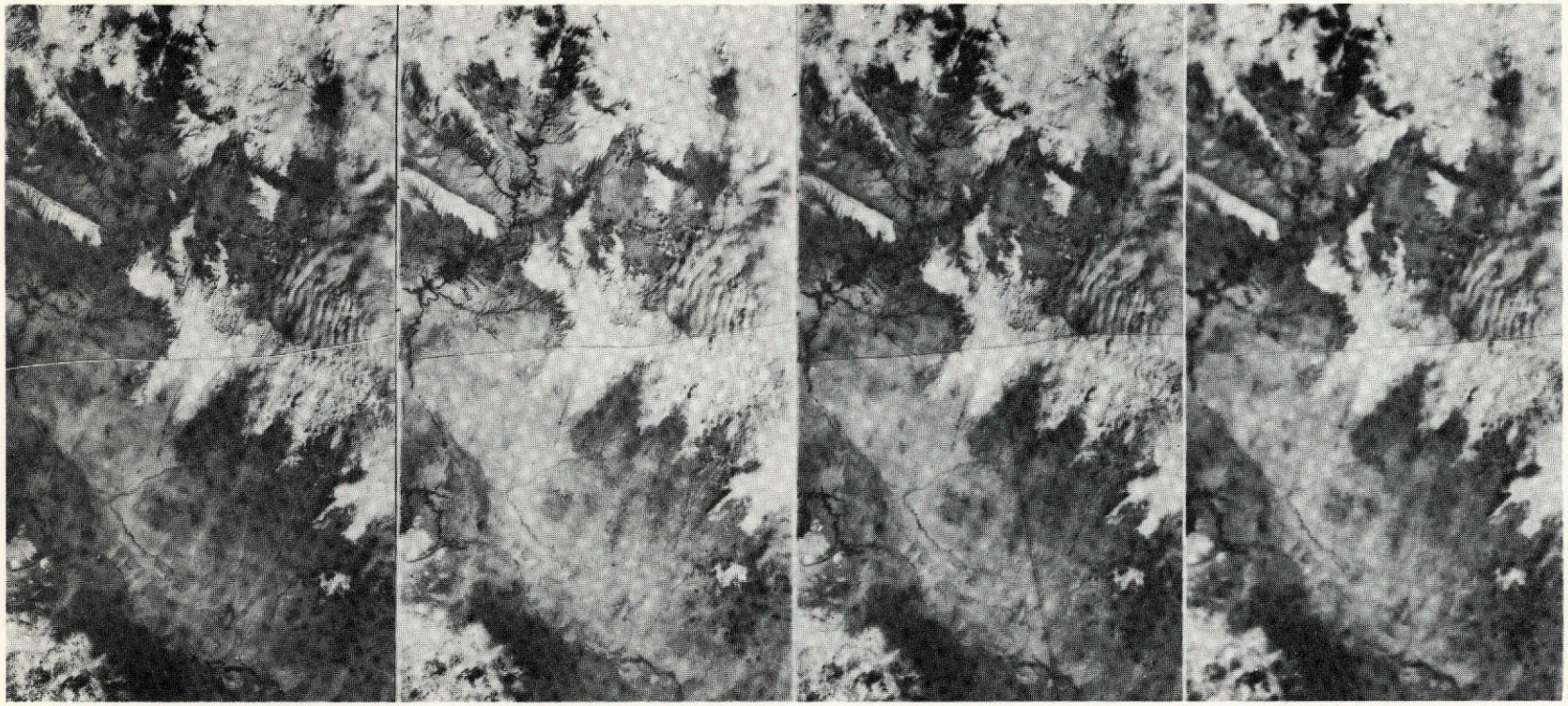

100 METER RESOLUTION | 1/8 nmi. RESOLUTION | 1/4 nmi. RESOLUTION | 1/2 nmi. RESOLUTION

Figure 3.19. Frames 1121-17324-17321

Figure A-7 shows the original, the 1/8 nmi, the 1/4 nmi, and the 1/2 nmi photographs. Note the cloud seeding effect caused by smoke plumes from Chicago. The wave structure in the clouds is still somewhat visible even at the 1/2 nmi resolution, although the structure has been severely degraded between the 1/4 and 1/2 resolution. However, the smoke plumes have disappeared. In the lower right hand corner of the frame the wave structure, which is perpendicular to the wave structure in the top of the frame, has disappeared in the 1/2 nmi photograph. It would be very difficult to distinguish the multi-layered structure near the top of the scene. Near the right hand edge of the scene in the 1/2 nmi photo, the cloud type would be difficult to recognize except for the fact that the cloud shadows are visible and could be measured.

3.2.8 Frames 1099-15184 through -15193 (Figure A-8)

These frames were taken on October 30, 1972, at the inlet to the Hudson Straight. The synoptic situation is shown in Figure 3.16. The strong low level northwesterly flow through the Straight is causing a band of strato-cumulus downstream of the Straight. It is already mature and in closed cellular form. This is caused by the relatively warm temperature of the water as compared to the land or air temperature. In the middle of the scene, note how the clouds are just beginning to form in small individual elements east of the coast and conform to the general outline of the coast approximately 70 nmi downstream. Newly formed ice appears as wisps offshore. Along the lower edge of the scene a deck of cirrostratus begins.

In the degraded images most of the information is still detectable. It is difficult to say if the cirrus would be recognized at 1/2 nmi resolution. It can be concluded that whereas the cloud deck is obviously cirrus at the original resolution, it probably could not be interpreted correctly at the 1/2 nmi resolution. The existence of the deck is still evidenced by the shadowed edge.

3.2.9 Frames 1182-16224, -16231 (Figure A-9 and 3.20)

This scene was taken over Hudson Bay on January 21, 1973. The cracks in the ice pack make it clearly distinguishable from the low stratus deck ($\approx$ 1200 ft.). This is still evident even in the 1/2 nmi resolution frame. The small wave structure in the clouds, however, is just barely detectable in the 1/8 nmi imagery, and not at all evident at the two lower resolutions.

Figures 3.21, 3.22, and 3.23 show the spectrum of image products available from the current operational meteorological program. Figure 3.21 is the hemispheric montage produced from the visible channel of the SR. (Individual digital elements are approximately 8 nmi at the latitude of interest.) This imagery is obviously only useful for macroscale analysis and forecasting of major systems. Figures 3.22 and 3.23 are, respectively, the visible and far infrared real time outputs from the VHRR. The different apparent brightness of the scene between the VHRR and MSS products is a result of the VHRR frame being acquired approximately 40 minutes earlier as well as the larger dynamic range

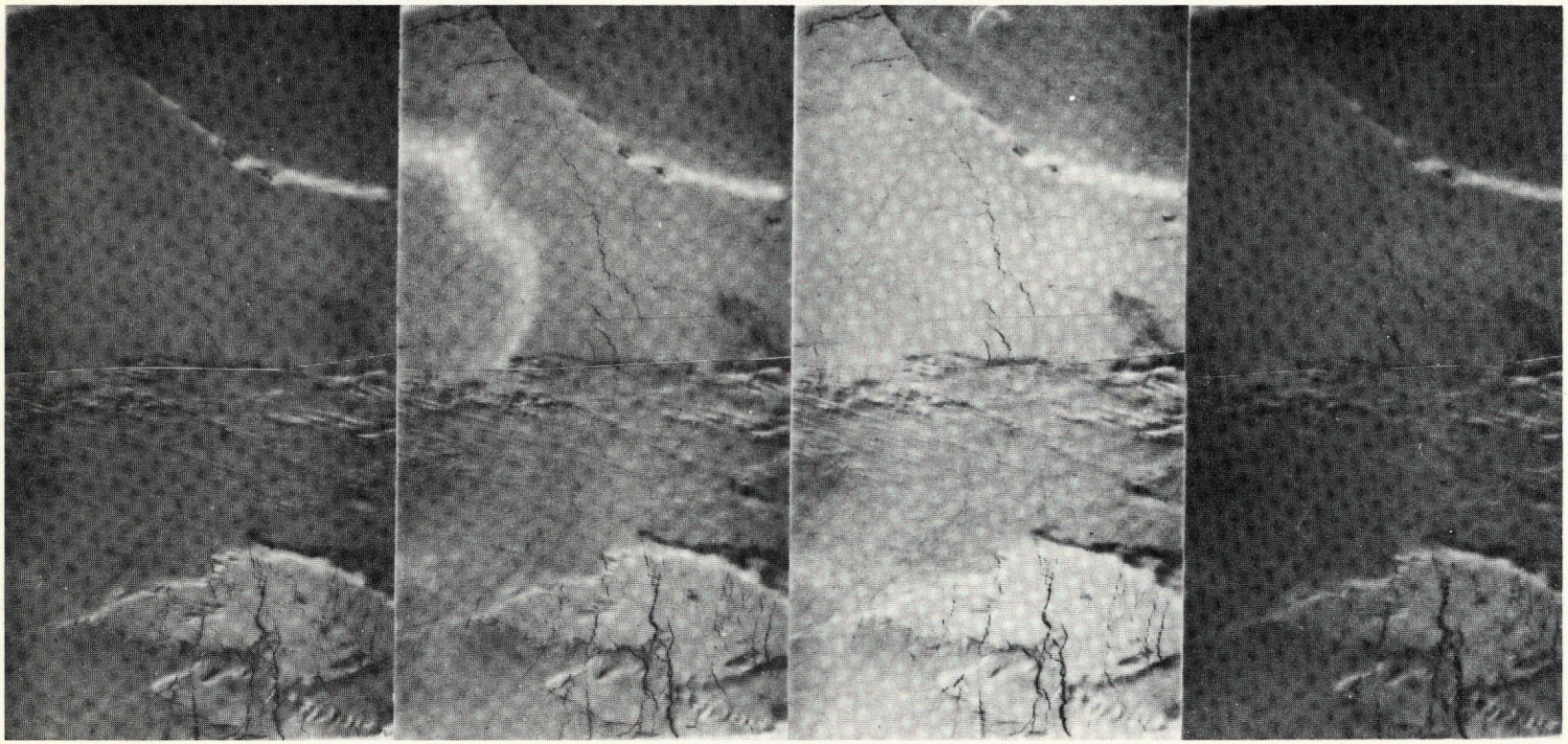

1/2 nmi.
RESOLUTION

1/4 nmi.
RESOLUTION

1/8 nmi.
RESOLUTION

100 METER
RESOLUTION

Figure 3.20. Frames 1182-16224-16231

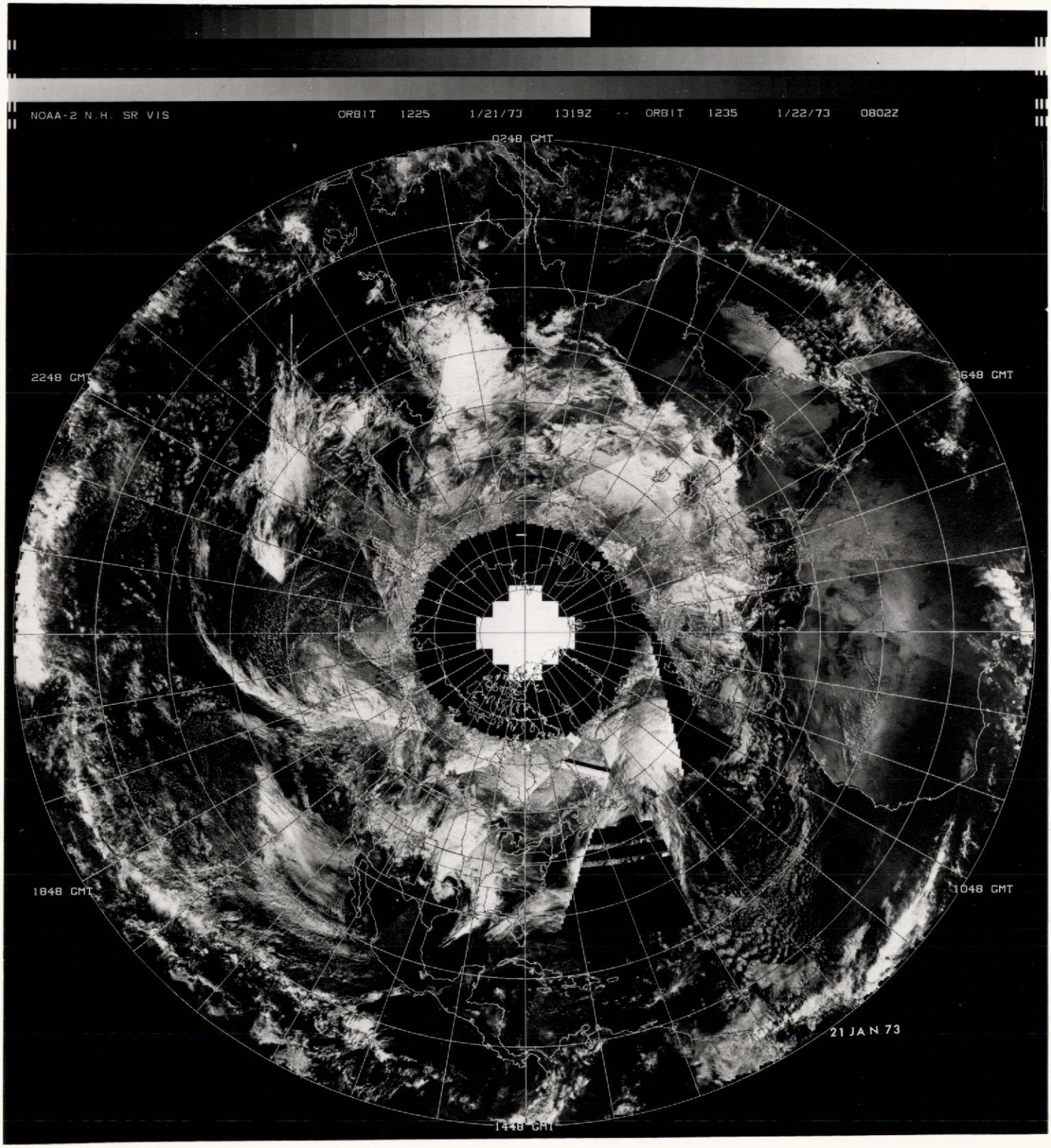

Figure 3.21. SR Hemispheric Montage (0.5 - 0.7μ)

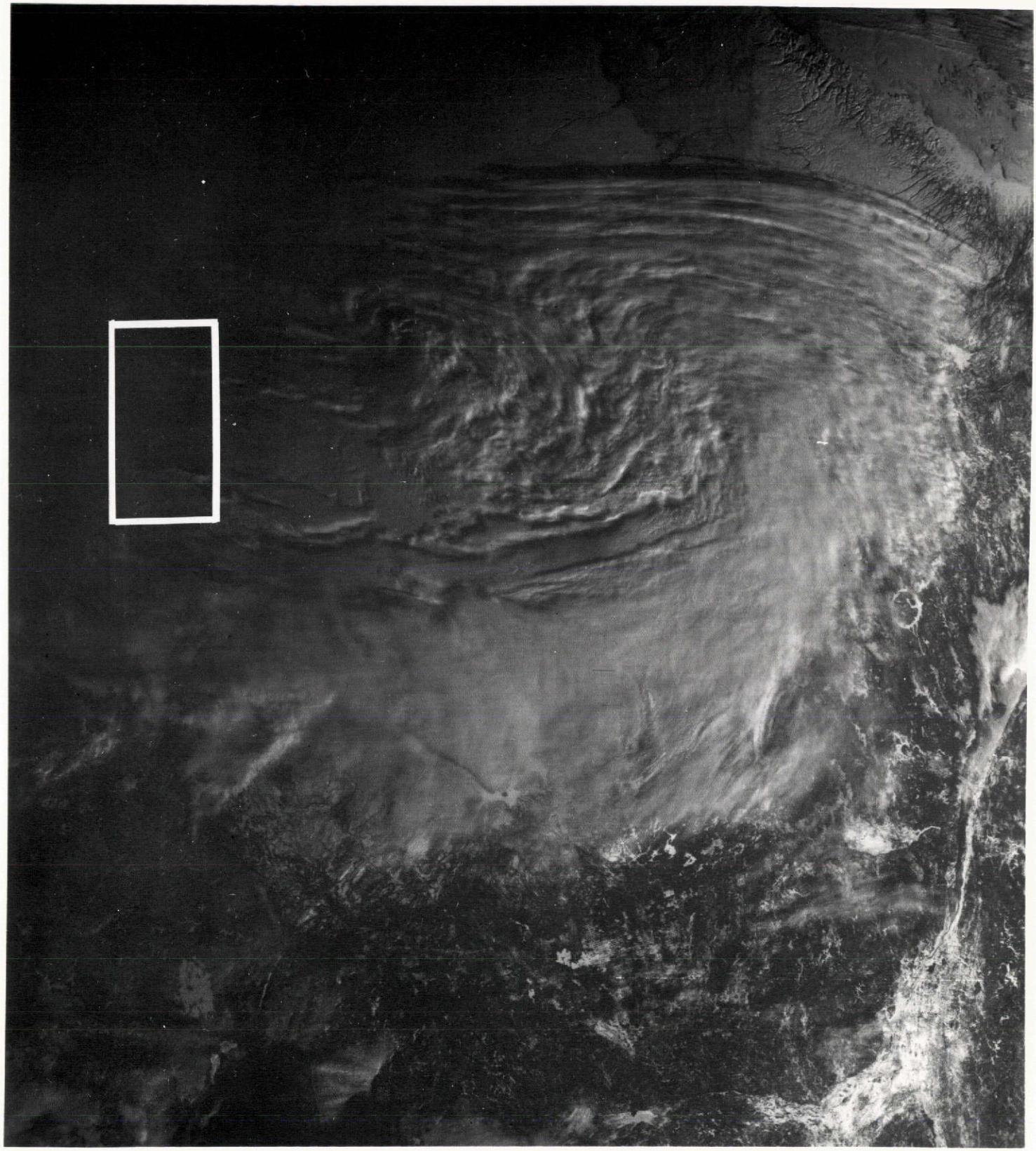

Figure 3.22. VHRR Image 21 Jan. 1973 (0.6 - 0.7μ)

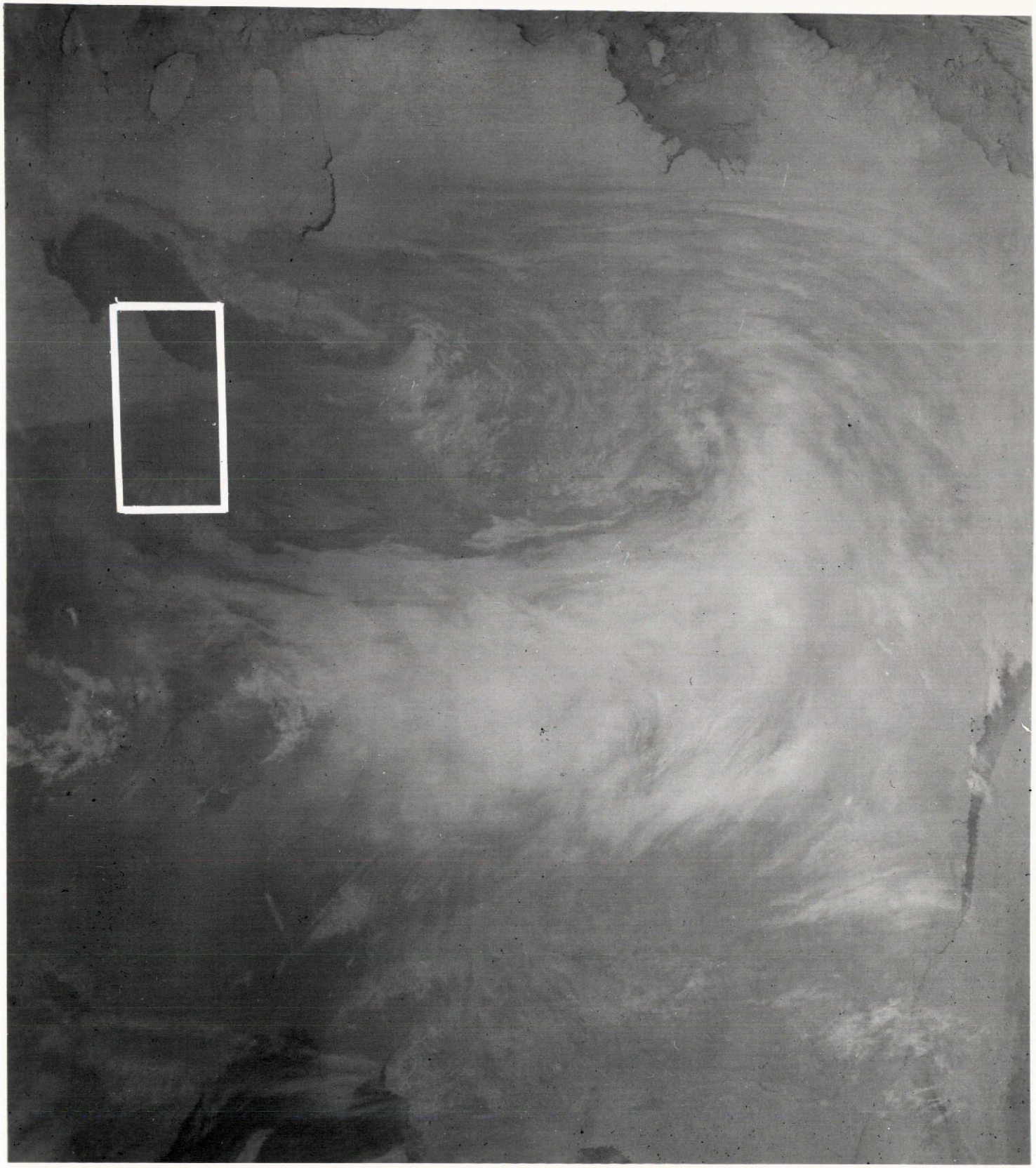

Figure 3.23. VHRR Image 21 Jan. 1973 (10.5 - 12.5μ)

of the VHRR. In fact, the reflected radiation is so low over the area of interest that little useful information can be gleaned from the image. However, in other areas of the image, ice, snow, and clouds are readily distinguishable. When both (visible and IR) images are analyzed together, a tremendous amount of information is available. Over the region of interest, the warmer stratus deck shows up well against the colder pack ice, indicating the strong low level inversion. Also, the warmer water, or thin ice, delineates the Hudson Bay shoreline. The layered nature of the cloudiness through the middle of the frame, is evident from the long shadows in the visible image and from the temperature difference in the IR image.

3.2.10 Frames 1088-16055, -16061 (Figure A-10)

This scene was taken over eastern Tennessee on October 19, 1972. The synoptic situation exhibited a large high centered over Iowa causing strong north-northwesterly low level winds over the scene. Here the cumulus cloud streets are aligned parallel to the wind at about 3700 feet altitude. Although many of the smaller cloud elements are lost and some of the streets are agglomerated in the degraded images, there is no difficulty determining the cloud type and cloud street orientation even in the 0.5 nmi image.

3.2.11 Frame 1173-15362 (Figure A-11)

This frame was taken on January 12, 1973, over southwestern Pennsylvania. A rapidly moving surface trough passed through this area on the afternoon of previous day. Snow showers accompanied the passage. The southernmost limit of the precipitation occurred in this area. Snow on the ground can be seen in the upper left corner of the frame and the tracks from the scattered snow showers can be seen horizontally across the frame. The stratocumulus clouds at about 2500 feet lie in rows perpendicular to the prevailing northwesterly wind. Even in the degraded frames all of the phenomena are clearly recognizable.

3.2.12 Frame 1173 (Figure A-12)

This scene was taken on October 19, 1972, over the lower portion of Lake Michigan. At the time the data was acquired, a large high pressure system was centered over Iowa. Weak northwesterly flow existed over the scene. There was, however, a definitive trough over this area at 850 mb. The result being the organized vortex exhibited by the stratocumulus cloud pattern ($\approx$ 3000 ft) in the scene.

In the degraded images the meso-scale vortex as well as the cloud type is still identifiable in the 0.5 nmi image.

3.2.13 Frames 1003-14485, -14482 (Figure A-13)

These frames were taken on July 26, 1972, over the north coast of New Brunswick, Canada. The scene contains many small fair weather cumulus clouds with an overlying veil of cirrus clouds which thickens towards the bottom of the scene. In the upper right, the cumulus clouds formed in streets along the low level wind direction. The wind direction is evidenced by the existence of the cumulus clouds over the water, where they would not naturally form because of the reduced heating. After the scene had been degraded to 0.5 nmi resolution, the cloud streets were still visible, but many of the smaller cumulus cells had lost their character. Also, the layered nature of the cloudiness towards the bottom of the scene lost its character. The interesting cloud formation just along the coast in the left center portion of the frame could be determined to be a very low stratus or fog deck when viewed at the original ERTS resolution because of the lack of shadows around the upper-left edges of the cloud formation. However, in the 0.25 and 0.5 nmi frames, there was nothing to distinguish it from several areas of coalesced cumulus cells.

In general, for this particular frame, little meteorological information was lost as a result of the resolution degradation from 100 meters to 0.25 nmi. Significant degradation just began to occur at 0.5 nmi.

3.2.14 Frame 1096-15092 (Figure A-14)

This frame was included for an example of a cumulonimbus. There is no anvil, but it does appear to have a cirrus cap. Saturation has occurred and a great deal of detail is probably lost. This is a good example of a confused sky where many scattered and broken cloud decks are occurring at several levels.

After degradation, this frame exhibits a tremendous variation in meteorological information between the 1/8 nmi and 1/2 nmi simulations. All of the cloud types and layers distinguishable in the original ERTS scene are also distinguishable at 1/8 nmi resolution. For the most part, this is also true at 1/4 nmi resolution. However, in the 1/2 nmi frame, little of the original cloud detail is present. The layered nature is absent in most places; the small fair weather cumulus are no longer recognizable and the many different types of middle level clouds have lost their individual character.

3.2.15 Frames 1062-15195, -15202 (Figure A-15)

This scene of North Carolina on September 23, 1972, shows the result of a large expanse of low level haze or high thin cirrus on the scene's contrast. A stationary front exists east-west along southern South Carolina. The low level flow across the scene is anti-cyclonically curved from the east. Mist is being reported under the stratocumulus deck in the northern portion of the scene. Thin cirrus is barely apparent along the coast at the bottom center of the scene.

In the degraded data, all of the information remains. Even the orientation of the cloud streets and the thin cirrus are clearly visible in the 1/2 nmi data.

3.2.16 Frames 1127-18064 through -18073 (Figure A-16)

The mountain snow in the Sierra Nevada range on November 27, 1972, is readily recognizable even at the 1/2 nmi resolution. For snow line mapping, however, the accuracy would probably increase greatly as the resolution was improved from 1/2, to 1/4, to 1/8 nmi. There would probably be little additional gain by going to the ERTS 100 meter resolution for this scene.

3.2.17 Frames 1010-20290 through -20295 (Figure A-17)

This scene shows ice in the Beaufort Sea on August 2, 1972. In the degraded 1/2 nmi scene, the existence of the low status deck is generally evident, but the wave structure does not become recognizable until the 1/4 nmi data is observed. A gradual agglomeration of the smaller ice floes occurs through the range of resolutions produced.

3.2.18 Frames 1004-16322, -16324 (Figure A-18)

This scene of ice in the extreme north portion of Hudson Bay on July 27, 1972, exhibits no significant change in information content when degraded to 1/2 nmi. At this resolution, the small floes have been replaced by a hazy appearance, but the outline of the ice field is still apparent.

3.2.19 Frames 1064-15324 through -15333 (Figure A-19)

This scene shows a highly dense cumulus cloud field over Florida/Georgia. The resolution degradation to 1/2 nmi has the effect of making the field appear to be much less densely populated. The organization of the cloud elements in the streets is barely detectable at the 1/2 nmi resolution.

3.2.20 Frames 1099-15211 through -15220 (Figure A-20)

This scene was also taken over Canada on October 30, 1972, about 65 minutes before the VHRR picture in Figure 3.15. The main change in the scene as the image is degraded occurs at 1/2 nmi where the cellular nature of the stratocumulus deck is beginning to disappear. (In the VHRR image the resolution is $\approx$0.85 nmi at Z.)

4.0 SPECTRAL INTERVAL UTILITY ANALYSIS

4.1 Experimental Methods

Analysis was completed on ten different MSS frames during this portion of the experiment. The effort consisted of selecting a variety of cloud types

and hydrologic features (e.g., ice, snow, streams, and lakes) over portions of terrain for use as reference backgrounds (e.g., vegetation, soil or rock surfaces).

For each of the selected frames, the original copy of the ERTS 70mm negative transparency received from NDPF was processed. For each scene, three different MSS filter bands were analyzed, vis. 0.5 to 0.6 millimicrometers (Band 4), 0.6 to 0.7mm (Band 5) and 0.8 to 1.1mm (Band 7).

Each of the scenes were annotated with reference ticks defining profiles across each frame for sampling density traces over features of interest.

The densitometer traces were analyzed to obtain radiance values and relative contrast for regions of interest. Care was taken to analyze only those areas where signal saturation did not occur.

The density measurements were performed on a Joyce/Loebl scanning microdensitometer. The measurement procedure followed on each frame consisted of reading and recording the calibration density wedge along the lower margins and then recording the density trace along a profile alignment. Both traces were plotted on the same sheet so as to facilitate the reading of radiance values for selected segments of imagery along the profile (sample shown in Figure 4.1).

The extraction of radiance values for the different scene elements was accomplished as follows: The density wedge, recorded on each ERTS frame, defines fifteen discrete grey levels representing radiance values ranging from zero radiance (white on the negative) to the maximum radiance (blackest step) for each particular band. To obtain a radiance value for a given feature in the scene (on the profile trace), a curve is first fitted to the trace of the ERTS grey scale recording. The plot was graphically generated on the densitometer so that the ordinate represents position along the profile and the abscissa depicts ascending values of radiance. Radiance value can be determined by relating a point (or an average swing) for a feature on the profile trace to its ordinate on the calibrated grey wedge curve (sample shown in Figure 4.2).

Aperture settings on the microdensitometer were kept constant for all readings with the exception of samples taken on one scene (Frame No. 1106-16042) showing aircraft contrails against water and over land. The standard aperture setting covered 0.12 X 0.13 mm or approximately 368 X 400 meters along the ground. For the contrail reading a smaller opening (0.09 X 0.08 mm, or 276 X 245 meters on the ground) was used to provide for higher signal discrimination when crossing the contrails along the profile trace.

From a tabulation of radiance values within a scene, calculations can be made to determine contrast between categories of meteorological items (i.e., clouds) or hydrological objects (i.e., ice) and their adjacent backgrounds. For example, clouds over water is computed by:

$$\text{Cloud/Water Contrast} = \frac{R_{AV}\ (\text{Clouds}) - R_{AV}\ (\text{Water})}{R_{AV}\ (\text{Water})}$$

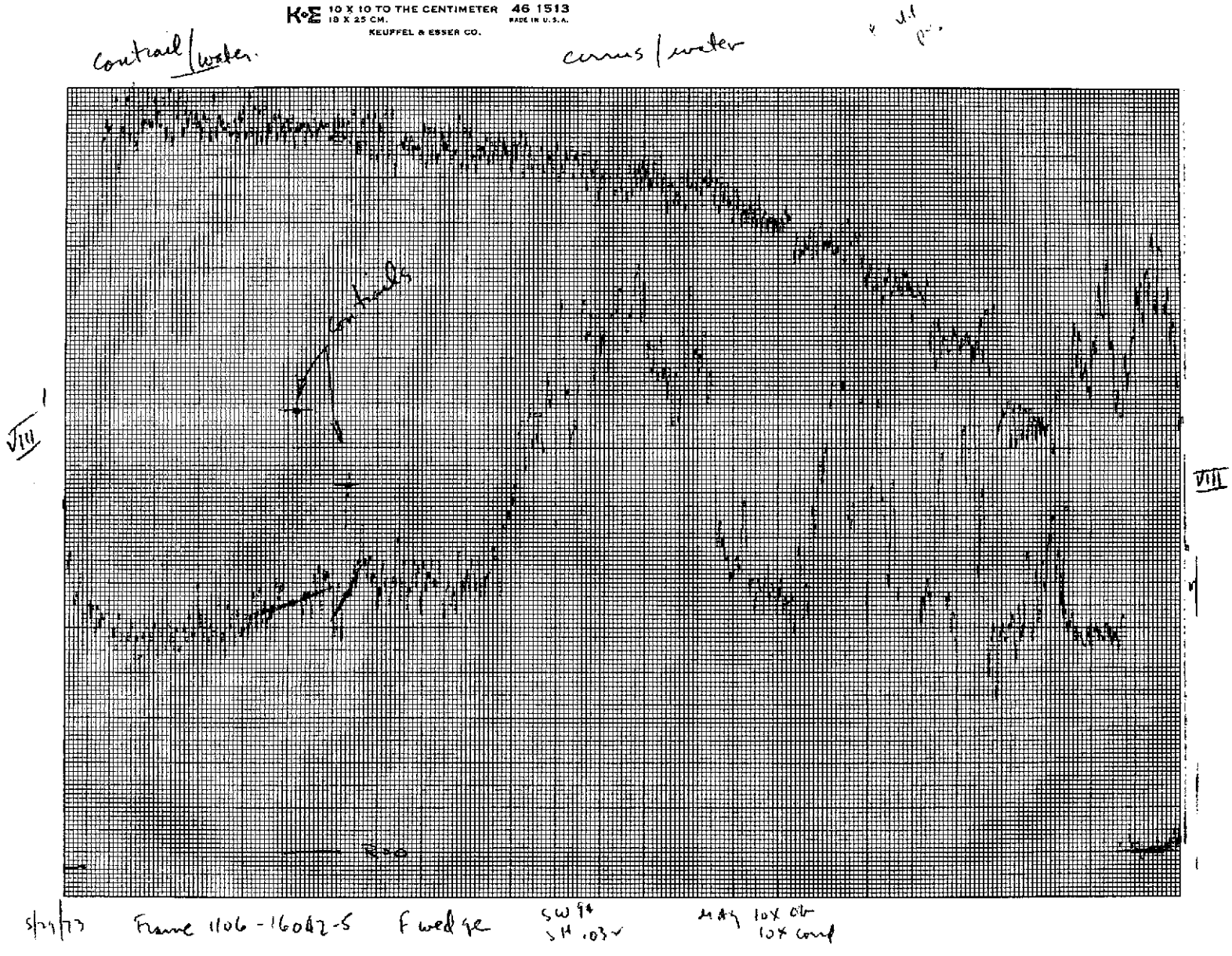

Figure 4.1 Densitometer Trace

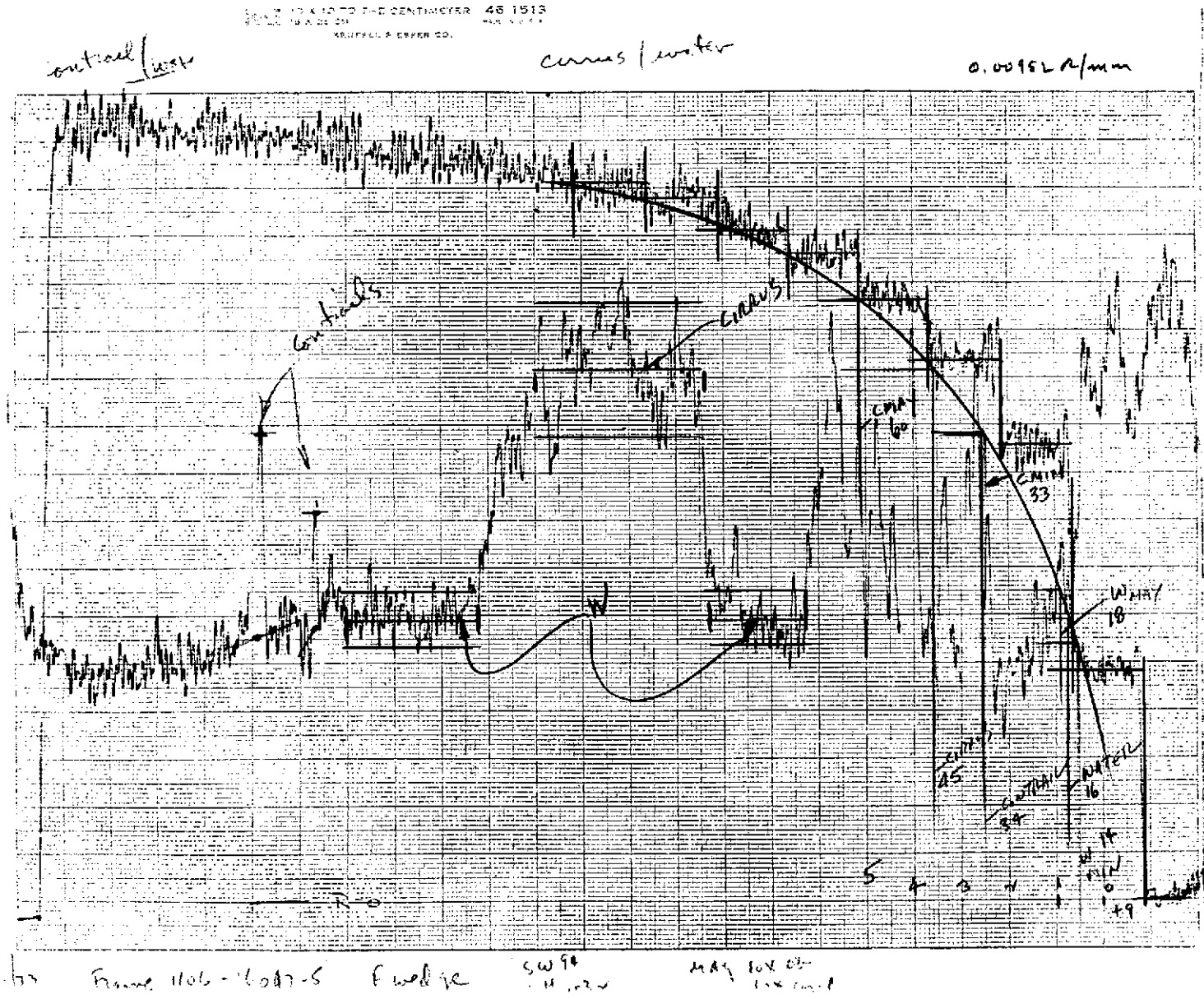

Figure 4.2 Densitometer Trace Worksheet

For each profile analyzed, a tabulation sheet was prepared upon which recordings are listed to show the scene type, a minimum and maximum reading (bounding that portion of the density trace which defines the scene type in question), and a reading of its average radiance value (sample shown in Figure 4.3). Each specimen type was processed in the three MSS bands used for this program, viz. Bands 4, 5, and 7.

In addition, contrasts were computed for the scene types versus backgrounds and are shown tabulated for the three filter bands on the right side of each sheet. A summary plot was compiled showing the contrast for typical met/hydro phenomena versus backgrounds. These serve to indicate variations in scene/background contrasts recorded through the different MSS filter bands.

Included within Figure 4.4 through Figure 4.13 are enlargements of the 70mm frames used in the analyses. For any given ERTS scene, profiles were aligned using scribed edge ticks on each of the 3 bands which were referenced to the same 'ground control' on all three frames on the same set. In this way profile readings on the microdensitometer were replicated over precisely the same trace on all three bands of any given scene.

4.2 Results

The measured values of radiance and contrast in the ten frames were used to support the comparison of two pairs of spectral intervals; 0.5 -0.6μ versus 0.6 - 0.7μ, and 0.6 - 0.7μ versus 0.8 - 1.1μ. The graph in Figure 4.14 shows the variation or contrast with spectral interval for a group of observations covering the range of meteorological phenomena measured in this experiment. Several different measurements were obtained for some of the categories. In those cases, a representative value was used in this graph.

The graph depicts the general results of the measurements made in this portion of the experiment:

(1) The measured contrast of a variety of cloud types in Band 5 (0.6 - 0.7μ) against land and water backgrounds was in each case more than one-and-one half times the contrast in Band 4 (0.5 - 0.6μ).

(2) While the high land/water contrast in Band 7 (0.8 - 1.1μ) was observed, the higher albedo of vegetation in Band 7 caused a reduced cloud/land contrast in Band 7 versus that in Band 5. For the cases measured, the quantitative result was that the cloud/land contrasts (where the land contained vegetation, i.e., not predominately desert or rock) in Band 5 (0.6 - 0.7μ) were in each case more than three times the contrast in Band 7 (0.8 - 1.1μ).

Qualitatively, it can be concluded that for observations of clouds, snow, and ice against any background, a 0.6 - 0.7μ channel provides more contrast and allows for better interpretability than a 0.5 - 0.6μ channel, or even a 0.5 - 0.7μ channel. Furthermore, the results of this experiment indicate that if information provided by a near-infrared channel is required, the combining of this energy with that in the visible region will result in a degradation of cloud/land contrasts.

K·E 10 X 10 TO ½ INCH 46 1473
7½ X 10 INCHES
KEUFFEL & ESSER CO

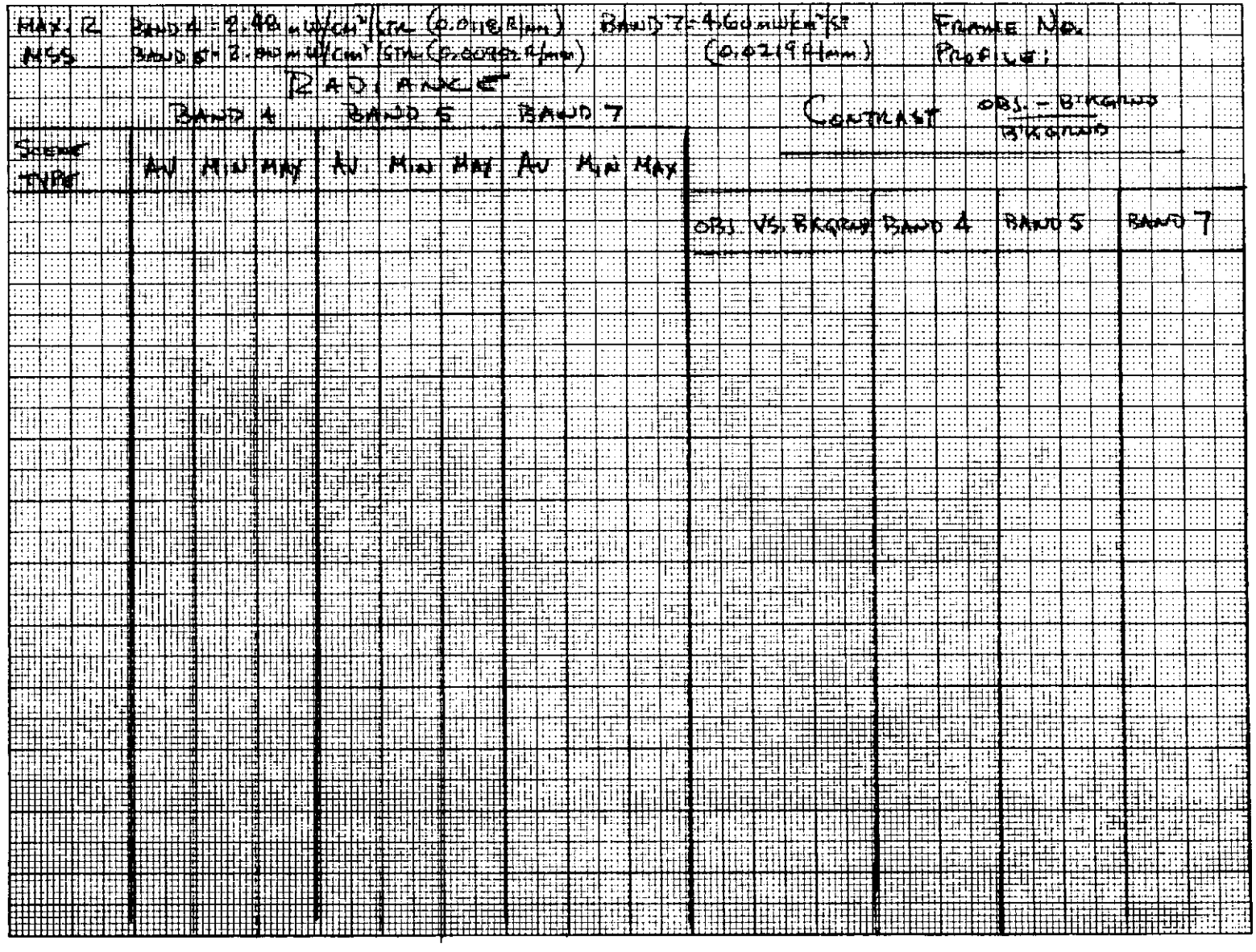

Figure 4.3 Radiance/Contrast Worksheet

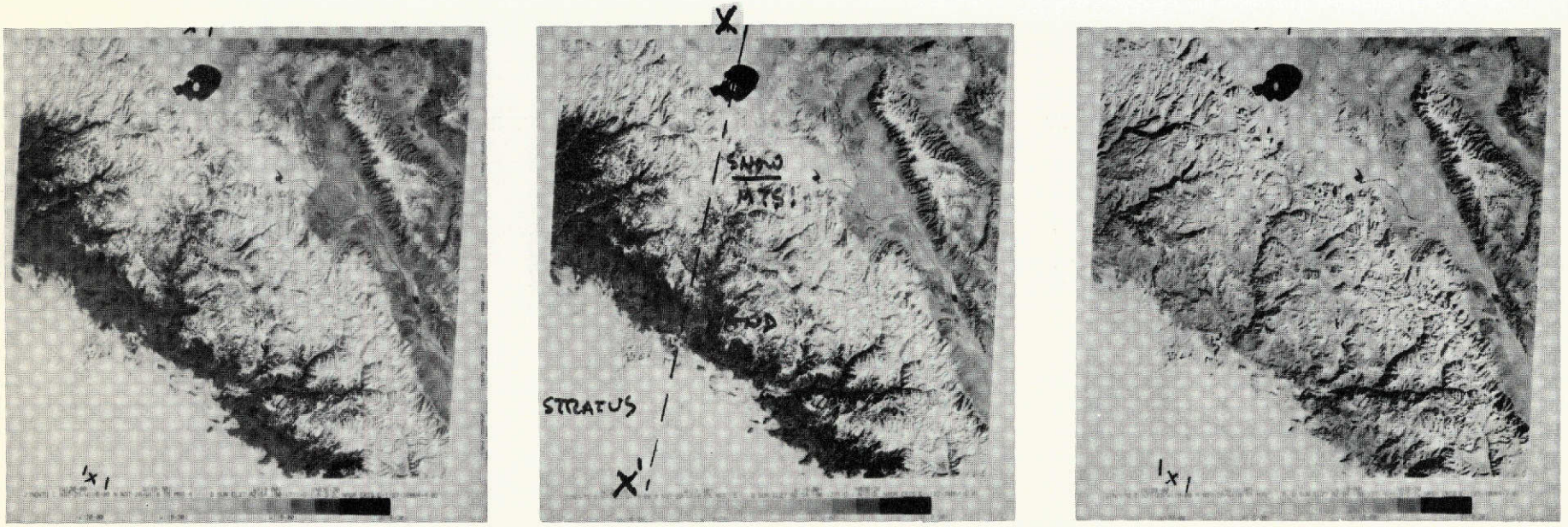

Figure 4.4. MSS Frame Used for Microdensitometer Recordings for Radiance & Contrast Measurement
- Clouds, Land, Mountain Snow -

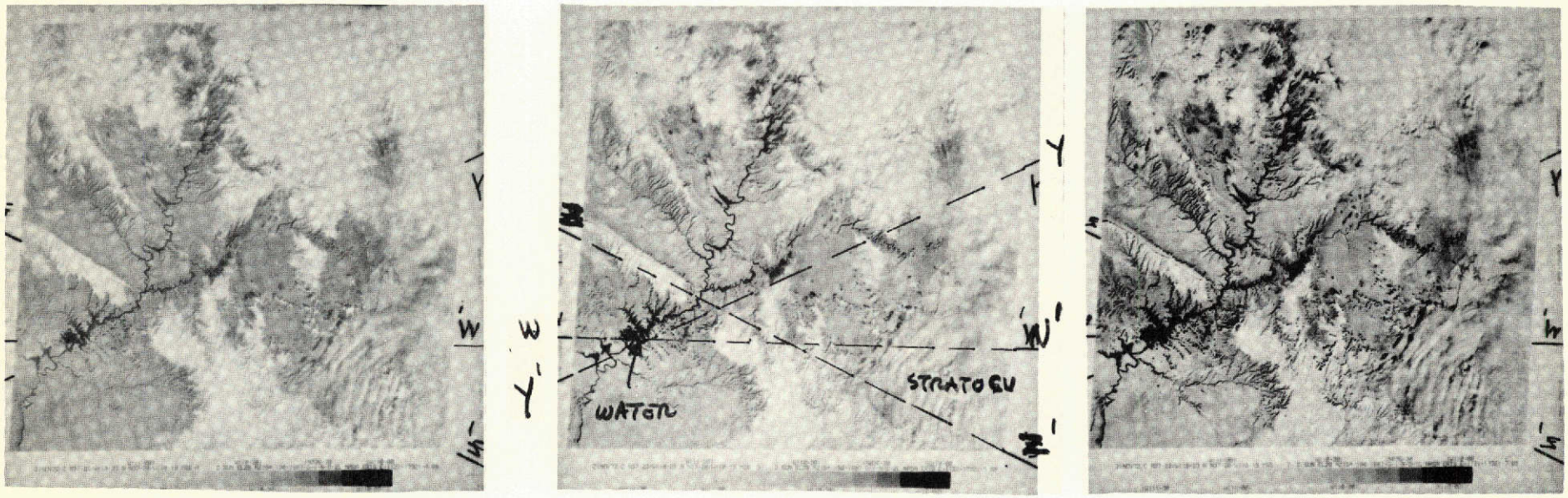

Figure 4.5. MSS Frame Used for Microdensitometer Recordings for Radiance & Contrast Measurement
- Clouds, Land, Lakes -

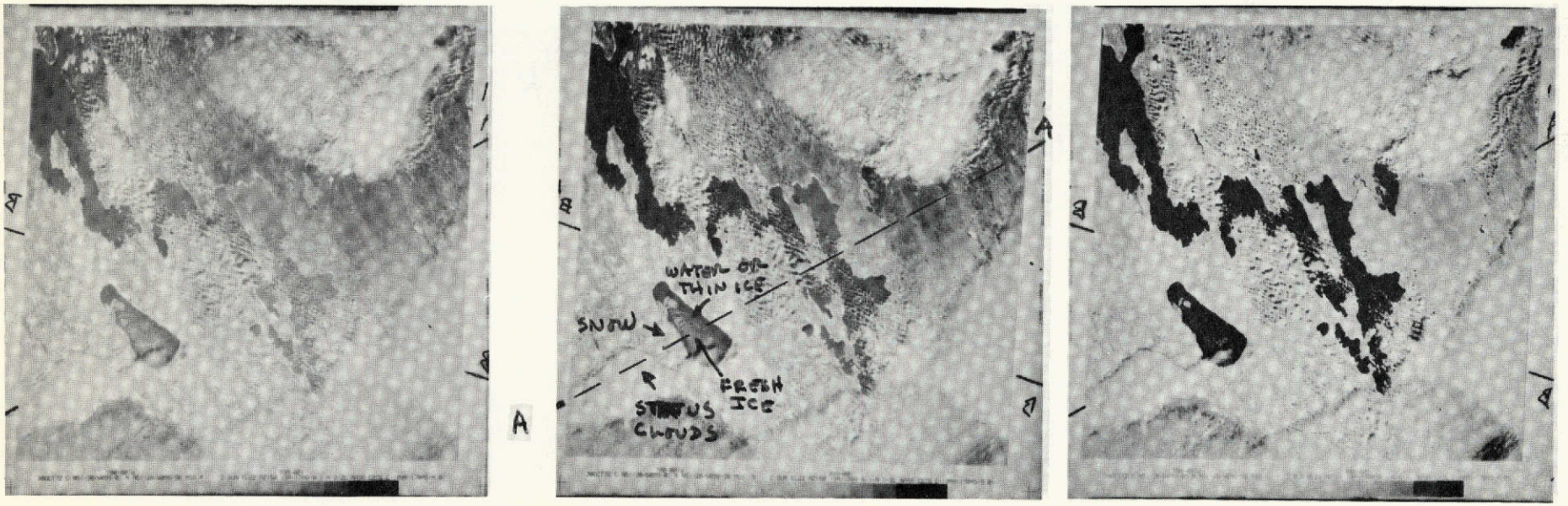

Figure 4.6. MSS Frame Used for Microdensitometer Recordings for Radiance & Contrast Measurement
- Clouds, Ice & Water -

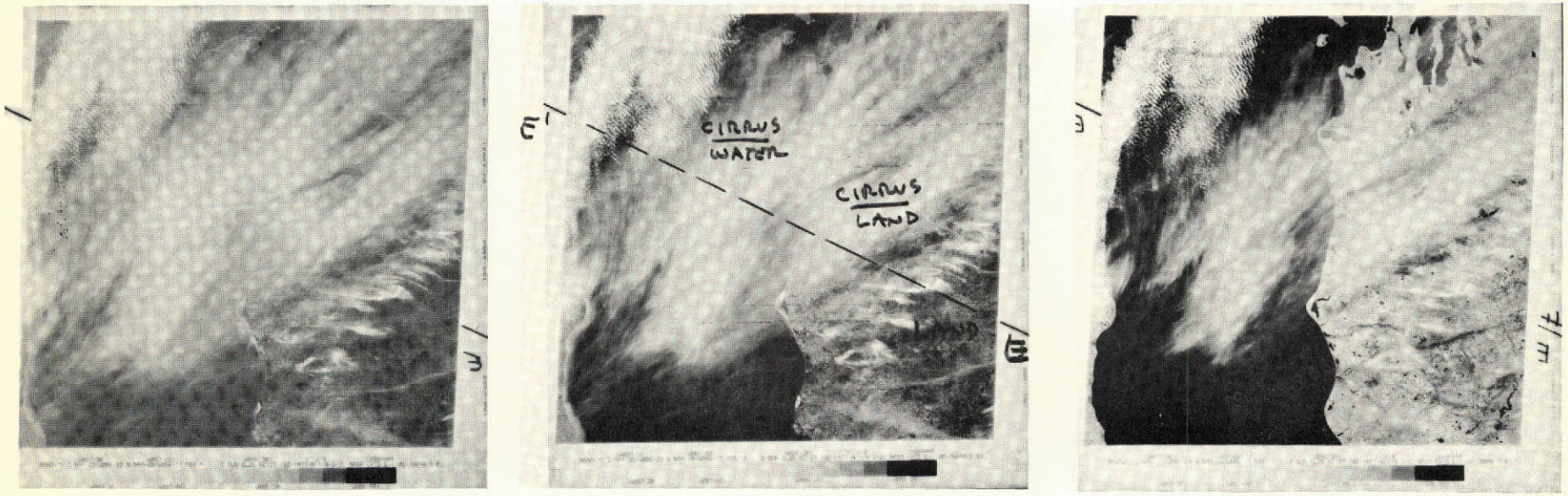

Figure 4.7. MSS Frame Used for Microdensitometer Recordings for Radiance & Contrast Measurement
- Cirrus Clouds/Land & Water -

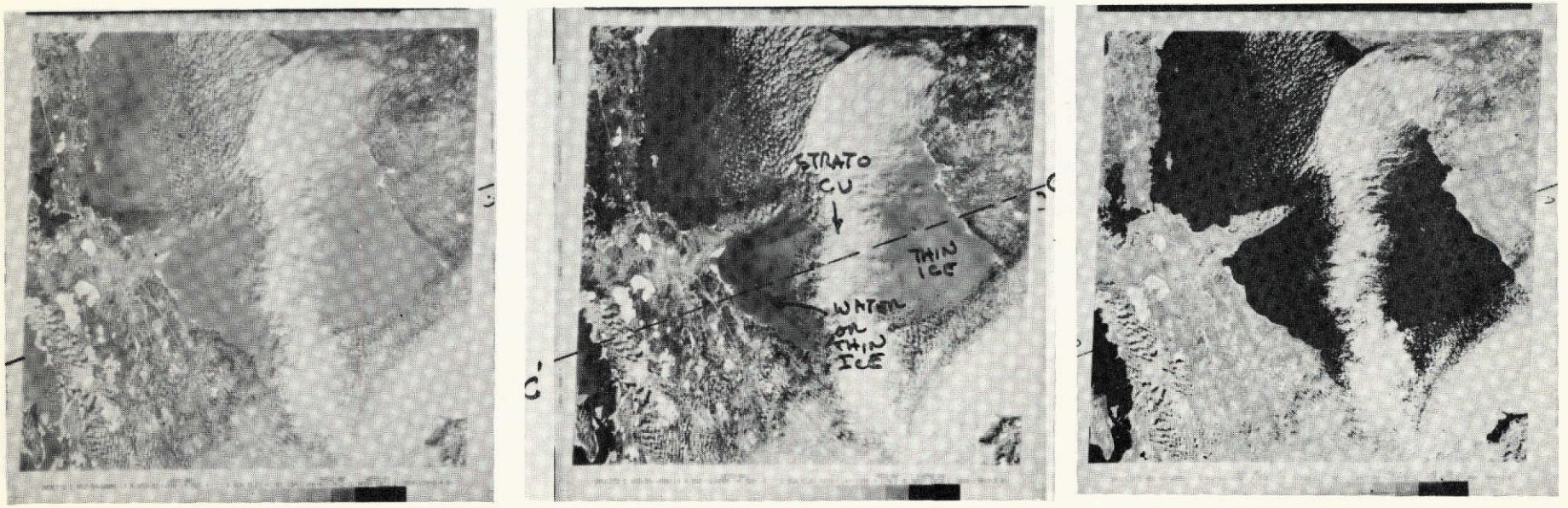

Figure 4.8. MSS Frame Used for Microdensitometer Recordings for Radiance & Contrast Measurement
- Clouds, New/Thin Ice -

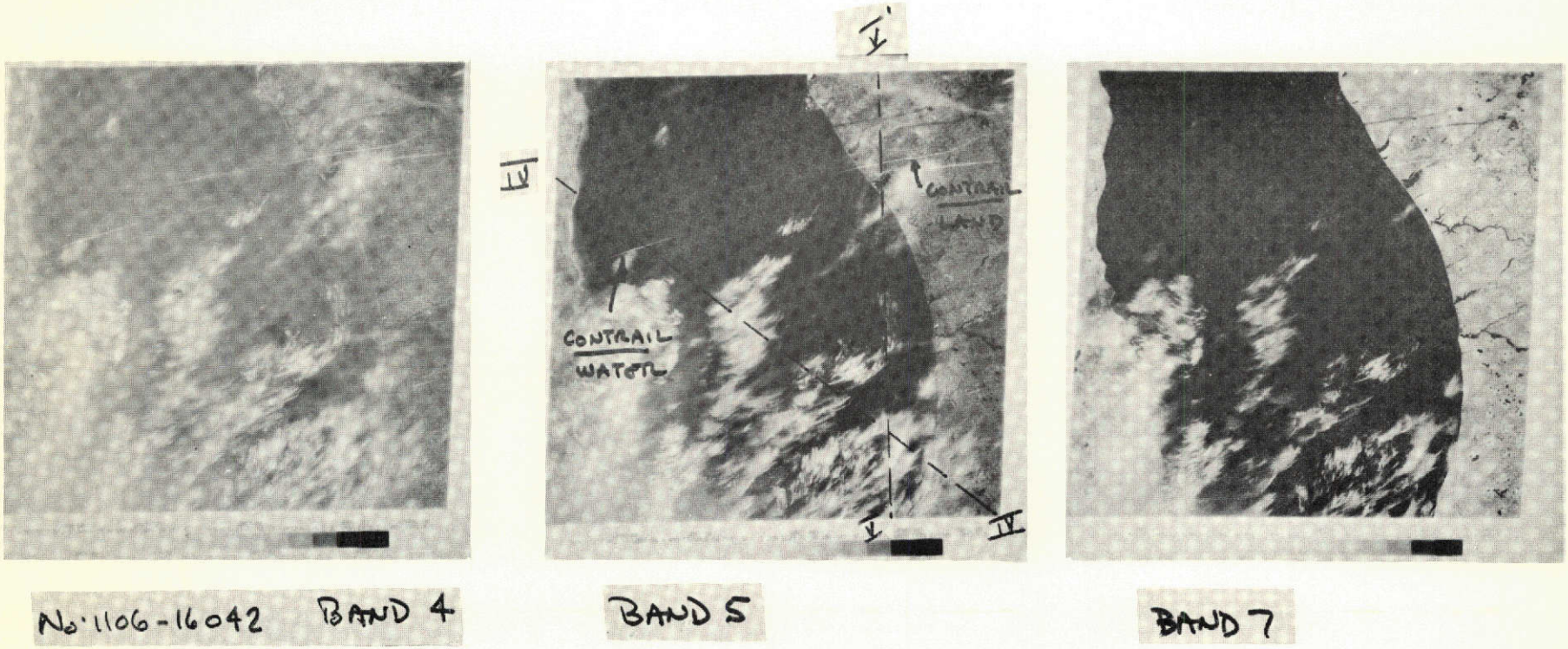

Figure 4.9. MSS Frame Used for Microdensitometer Recordings for Radiance & Contrast Measurement
- A/C Contrails Over Land/Water -

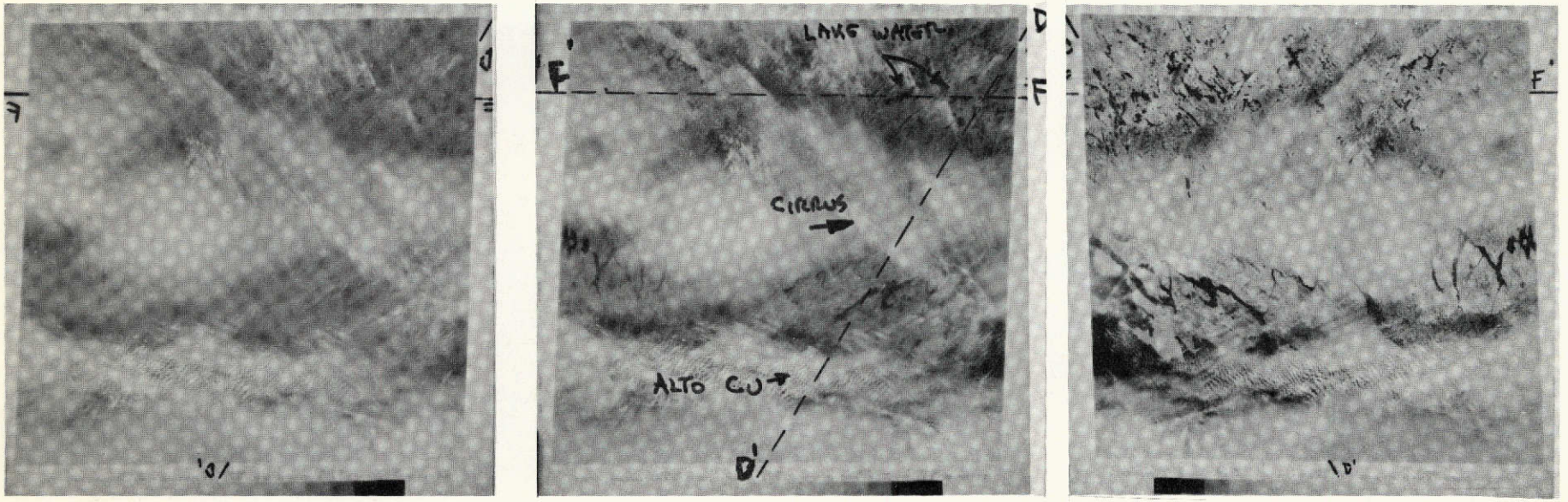

Figure 4.10. MSS Frame Used for Microdensitometer Recordings for Radiance & Contrast Measurement
- Clouds/Land & Water -

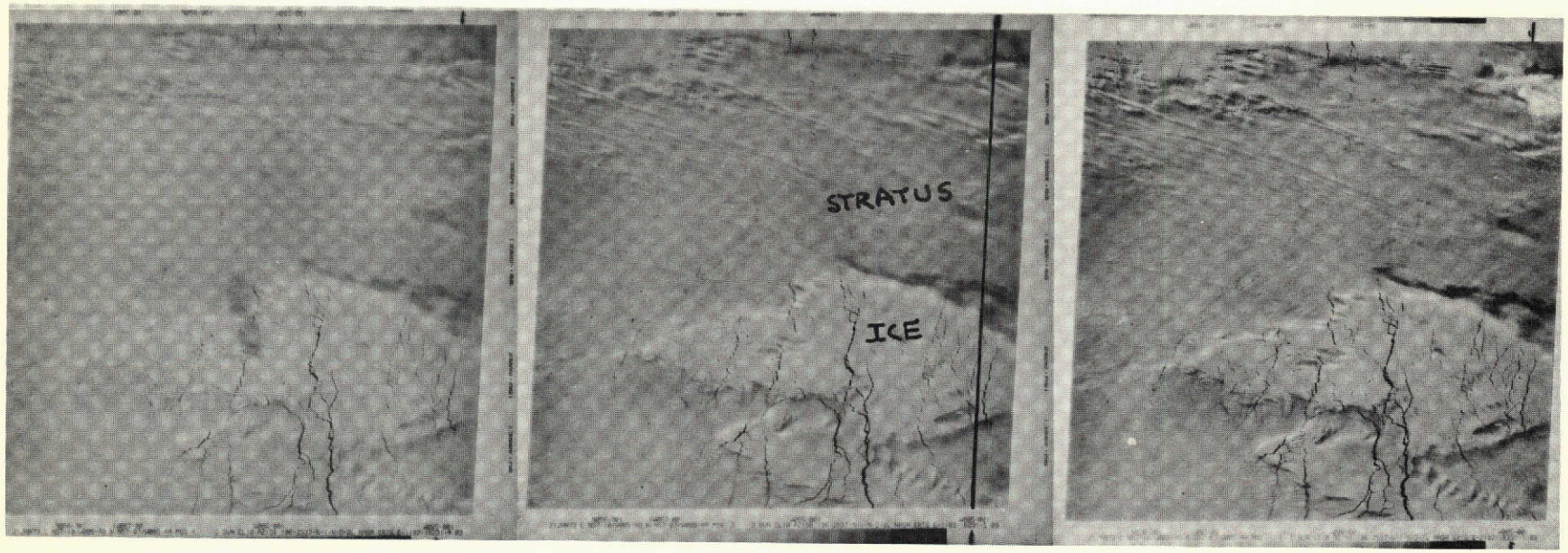

FRAME NO: 1182 - 16241 - BAND 4 FRAME NO: 1182 - 16241 - BAND 5 FRAME NO: 1182 - 16241 - BAND 7

Figure 4.11. MSS Frame Used for Microdensitometer Recordings for Radiance and Contrast Measurements - Stratus, Ice -

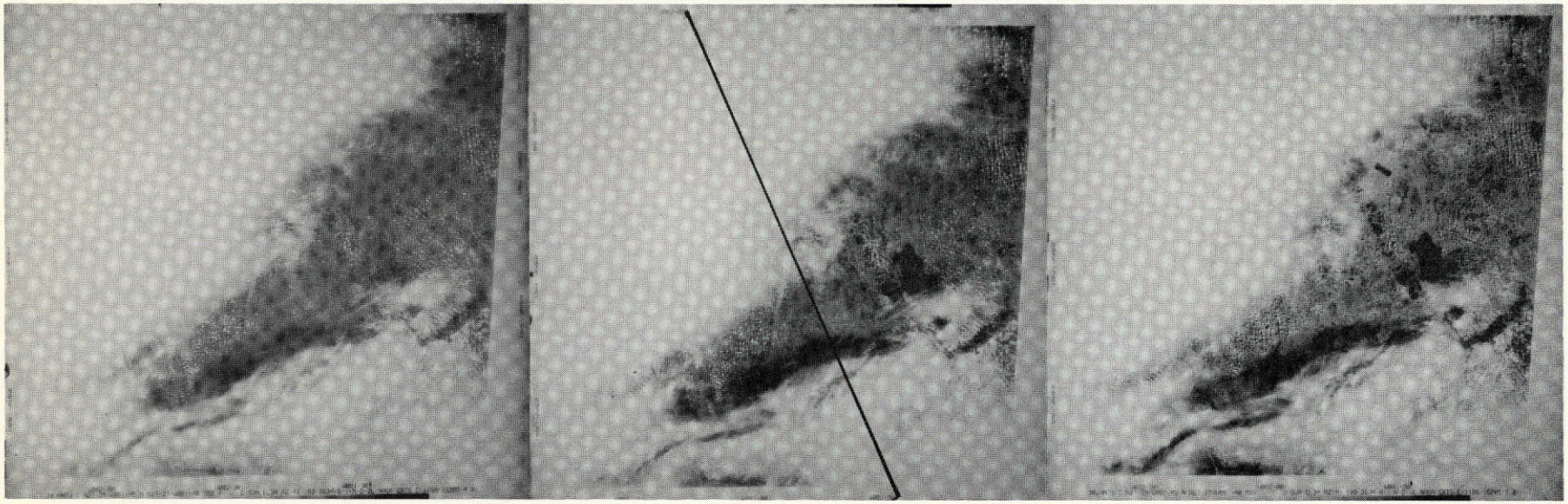

FRAME NO: 1189 - 15285 - BAND 4 FRAME NO: 1189 - 15285 - BAND 5 FRAME NO: 1189 - 15285 - BAND 7

Figure 4.12. MSS Frame Used for Microdensitometer Recordings for Radiance and Contrast Measurements - Clouds, Land -

FRAME NO: 1096 - 15092 - BAND 4 FRAME NO: 1096 - 15092 - BAND 5 FRAME NO: 1096 - 15092 - BAND 7

Figure 4.13. MSS Frame Used for Microdensitometer Recording for Radiance and Contrast Measurements - Clouds, Water -

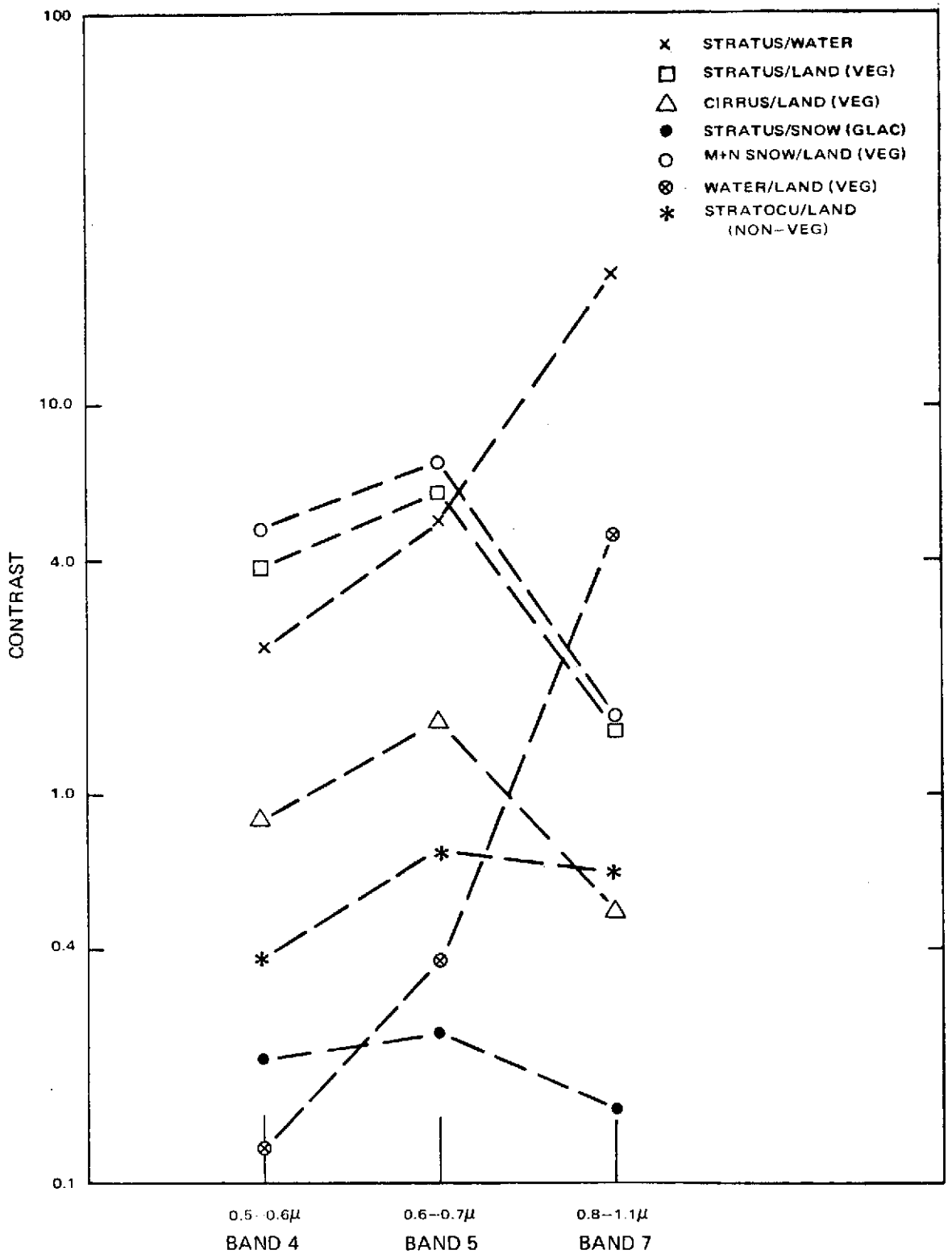

Figure 4.14 Graph of Contrast vs Spectral Band

It was difficult to find representative qualitative values for combinations of cloud/ice and cloud/snow. Discrimination in these cases is usually made by observation of internal structure and not on the basis of contrast. In fact both positive and negative contrasts (though small in absolute values) were measured for each of these cases.

The following table is a summary of the valid measurements obtained.

TABLE 4.1. MEASURED CONTRASTS - MSS IMAGERY

Observation	Contrast		
	Band 4	Band 5	Band 7
stratus/snow (glacier)	0.21	0.24	0.15
New lake ice/water	0.27	0.39	2.50
stratocu/new lake ice	2.39	3.07	17.20
altocu/land	0.69	1.13	0.22
thin cirrus/land	1.18	3.00	0.54
altocu/water	1.43	7.49	>100
thin cirrus/water	1.65	7.65	>100
thin cirrus/land	0.89	1.50	0.74
contrail/land	0.40	0.68	0.46
contrail/water	0.57	1.12	1.00
cirrus/water	0.81	1.81	3.80
mtn. snow/land	4.83	7.07	1.56
stratus/land	3.86	5.99	1.43
stratocu/land (non-veg)	0.38	0.72	0.62
land (non-veg)/water	0.47	0.98	3.05
altocu/water	0.41	0.56	3.10
contrail/water	0.32	0.64	5.20
water/cloud shadow	0.18	0.38	0.25
land/cloud shadow	0.45	0.92	2.25
pack ice/cloud shadow	0.68	0.87	1.65

APPENDIX A

CATALOG OF DEGRADED MSS SCENES

This catalog is composed of the ERTS MSS Band 5 (0.6 - 0.7μ) scenes which were degraded during the resolution reduction portion of the experiment. The analysis of each scene is summarized in Section 3.2 of this report, with the appendix figure number referenced in the title of the corresponding subsection.

The scenes are presented in mosaic 70mm format as 6th generation positive transparencies. The format for each figure is the same.* The scene on the extreme left of each figure is a copy of the original ERTS MSS 70mm data. Moving from left to right across the figure, the original scene is followed in order by the simulation of data acquired by a radiometer with a 1/8 nmi IFOV, a 1/4 nmi IFOV, and finally, at the extreme right side of the figure, a 1/2 nmi IFOV.

The difference in information content in the various simulations can best be seen by viewing the scenes in order of increasing resolution from 1/2 nmi to 100 meters.

*With the exception of Figure A-2A and A-2B which are annotated appropriately.